

Suppression of internal waves by thermohaline staircases

Timour Radko†

Department of Oceanography, Naval Postgraduate School, Monterey, CA 93943, USA

(Received 27 December 2019; revised 30 June 2020; accepted 3 July 2020)

This study attempts to quantify and explain the systematic weakening of internal gravity waves in fingering and diffusive thermohaline staircases. The interaction between waves and staircases is explored using a combination of direct numerical simulations (DNS) and an asymptotic multiscale model. The multiscale theory makes it possible to express the wave decay rate (λ_d) as a function of its wavenumbers and staircase parameters. We find that the decay rates in fully developed staircases greatly exceed values that can be directly attributed to molecular dissipation. They rapidly increase with increasing wavenumbers, both vertical and horizontal. At the same time, λ_d is only weakly dependent on the thickness of layers in the staircase, the overall density ratio and the diffusivity ratio. The proposed physical mechanism of attenuation emphasizes the significance of eddy diffusion of temperature and salinity, whereas eddy viscosity plays a secondary role in damping internal waves. The asymptotic model is successfully validated by the DNS performed in numerically accessible regimes. We also discuss potential implications of staircase-induced suppression for diapycnal mixing by overturning internal waves in the ocean.

Key words: double diffusive convection

1. Introduction

Perhaps the most spectacular and intriguing effect realized in multicomponent fluids is the spontaneous formation of a series of relatively well-mixed layers vertically separated by sharp interfaces, known as thermohaline staircases (Schmitt 1994; Kelley *et al.* 2003; Radko 2013). The origin of staircases has been linked to double-diffusive convection, broadly defined as a combination of processes driven by dissimilar diffusivities of density components (Stern 1960). While double-diffusive convection occurs in numerous astrophysical, geophysical and engineering systems (e.g. Turner 1985; Radko 2013; Garaud 2018) our focus is on the ocean, where density is largely controlled by the temperature and salinity of sea water. Most double-diffusive phenomena, including thermohaline staircases, can be classified into two distinct categories: fingering and diffusive. The fingering (diffusive) regime is realized when relatively salty and warm fluid is located above (below) cold and fresh.

The interest of the oceanographic community in the dynamics and transport characteristics of thermohaline staircases, both fingering and diffusive, is not limited to mere intellectual curiosity. Staircases are often associated with elevated rates of diapycnal

† Email address for correspondence: tradko@nps.edu

mixing, which in turn can influence the ocean's ability to transport heat, salt, nutrients, pollutants and carbon dioxide. For instance, field measurements in the fingering Caribbean staircase reveal an increase in vertical mixing by an order of magnitude relative to analogous smooth-gradient regions (Schmitt *et al.* 2005). The salt flux through this staircase alone exceeds the net turbulent transport by overturning gravity waves – another primary source of small-scale mixing – throughout the entire North Atlantic subtropical thermocline. It also becomes increasingly clear that diffusive staircases, which are more common in high-latitude oceans, can substantially influence polar climate and large-scale circulation patterns (e.g. Turner 2010; Polyakov *et al.* 2017; Bebieva & Speer 2019). Low levels of internal wave energy and the abundance of staircases in the interior of the Arctic Ocean (e.g. Guthrie, Morison & Fer 2013; Guthrie, Fer & Morison 2015) imply that double diffusion by default dominates vertical mixing in the halocline. As a result, staircases in the upper Arctic act as a bottleneck for heat transport from the relatively warm and salty waters of Atlantic origin and the overlying colder and fresher water-masses, motivating efforts to fully understand their dynamics and properties (e.g. Radko 2019a).

There have been numerous attempts to evaluate mixing rates that can be attributed directly to staircases using observations (e.g. Schmitt *et al.* 2005; Veronis 2007; Timmermans *et al.* 2008), theoretical models (e.g. Linden & Shirtcliffe 1978; Kelley 1990; Worster 2004), laboratory experiments (e.g. Fernando 1989; Krishnamurti 2009) and simulations (e.g. Carpenter, Sommer & Wuest 2012; Flanagan, Lefler & Radko 2013). The focus of the present investigation, however, lies in a different direction – the interaction between staircases and internal waves. It is generally accepted that a substantial fraction of small-scale mixing in the ocean can be attributed to wave overturns (e.g. Thorpe 2005). Thus, it is possible that staircases also indirectly influence the net diapycnal mixing by controlling the intensity and spectrum of internal waves in their vicinity.

In this regard, it should be mentioned that the dynamics and consequences of the interaction between waves and double-diffusive processes are highly configuration dependent. For instance, one of the earliest results in this area was the discovery of collective instability by Stern (1969). The term collective instability represents the spontaneous amplification of internal waves in smooth finger-favourable stratification. Stern's model was later refined and generalized by Holyer (1981, 1985), Stern, Radko & Simeonov (2001) and Traxler *et al.* (2011). On the other hand, laboratory studies of Ruddick (1980, 1985) reveal rapid damping of standing internal waves in layered fingering stratification. Direct numerical simulations (Stellmach *et al.* 2011) demonstrate that the initial growth of internal waves – caused by collective instability – is promptly reversed after the spontaneous development of staircases. The recent studies of the transmission and reflection of remotely generated internal waves by staircases (Ghaemsaidi *et al.* 2016; Sutherland 2016; Wunsch 2018) also point to the adverse impact of staircases on waves.

Our motivation to further investigate wave–staircase interactions is twofold. The first and foremost is our belief that the physical mechanism of wave–staircase interactions has not been fully explained yet. Key unresolved questions concern the roles of the eddy transfer of momentum and buoyancy, the relative significance of microscale (~ 1 cm in the ocean) and fine-scale ($\sim 1 - 10$ m) processes and the precise identification of the chain of events leading to the suppression of internal waves. The second item on our wish list is the complete exploration of the relevant parameter space, which includes the variation in the height of steps, thickness of interfaces, background parameters and wavenumbers. The present-day computational constraints preclude the direct numerical simulation (DNS) based investigation of many regimes realized in the ocean even in two dimensions. Therefore, a more feasible approach – and the one adopted in this work – involves the development of a simplified analytical model for the wave decay rate as a

function of all relevant parameters and its validation by DNS in the numerically accessible regimes.

Our study attempts to address these challenges using techniques of the multiscale homogenization theory (e.g. Meshalkin & Sinai 1961; Manfroi & Young 1999, 2002; Balmforth & Young 2002, 2005). Multiscale mechanics is a broad and active field and its methods are now commonly used in numerous fluid dynamical applications. A review of fundamentals and principal advancements in this area can be found, for instance, in Mei & Vernescu (2010). Multiscale theories, including the present model, generally assume an analytical small-scale pattern and analyse its interaction with larger-scale structures (e.g. Gama, Vergassola & Frisch 1994; Novikov & Papanicolau 2001; Radko 2011) using two sets of spatial and temporal scales. Theoretical development is based on the asymptotic expansion in powers of a small parameter (ϵ) representing the ratio of the assumed small and large spatial scales. Sequentially solving a series of balanced equations arising at each order in ϵ makes it possible to formulate explicit large-scale equations. Using the multiscale method, we analyse the evolution of large-scale (relative to the staircase layer height) internal waves in layered stratification. In all cases considered, we find that the staircases systematically suppress internal waves. The explicit and dynamically transparent nature of the multiscale model makes it possible to unambiguously interpret the essential physics at play.

The manuscript is organized as follows. In § 2, we formulate the problem and introduce governing equations. Section 3 presents preliminary DNS which illustrate the suppression of internal waves by diffusive and fingering staircases. The multiscale model representing this interaction is described in § 4. In § 5, we validate the multiscale theory by DNS and explore the relevant parameter space. The potential oceanographic implications of our findings are discussed in § 6. We draw conclusions and summarize the results in § 7.

2. Formulation

The temperature and salinity fields (T_{tot}^*, S_{tot}^*) are separated into linear vertical background profiles (T_{bg}^*, S_{bg}^*) and a departure (T^*, S^*) from them

$$\left. \begin{aligned} T_{tot}^* &= T_{bg}^* + T^* = A_T z^* + A_{T0} + T^* \\ S_{tot}^* &= S_{bg}^* + S^* = A_S z^* + A_{S0} + S^* \end{aligned} \right\}, \quad (2.1)$$

where (A_T, A_{T0}, A_S, A_{S0}) are constants. The asterisks hereafter denote dimensional quantities and the subscripts ‘*tot*’ represent the total field variables. The configuration in which background temperature and salinity decrease upward ($\partial T_{bg}^*/\partial z^* = A_T < 0$ and $\partial S_{bg}^*/\partial z^* = A_S < 0$) is referred to as diffusive stratification. The fingering stratification, on the other hand, is realized in regions where $A_T > 0$ and $A_S > 0$. The governing system used in this study is based on the incompressible Boussinesq approximation in two dimensions and the linear equation of state. It is expressed in terms of perturbation variables (T^*, S^*) as follows

$$\left. \begin{aligned} \frac{\partial T^*}{\partial t^*} + \mathbf{v}^* \cdot \nabla T^* + w^* \frac{\partial T_{bg}^*}{\partial z^*} &= k_T \nabla^2 T^* \\ \frac{\partial S^*}{\partial t^*} + \mathbf{v}^* \cdot \nabla S^* + w^* \frac{\partial S_{bg}^*}{\partial z^*} &= k_S \nabla^2 S^* \\ \frac{\partial \mathbf{v}^*}{\partial t^*} + \mathbf{v}^* \cdot \nabla \mathbf{v}^* &= -\frac{1}{\rho_0^*} \nabla p^* + g(\alpha T^* - \beta S^*) \mathbf{k} + \nu \nabla^2 \mathbf{v}^* \\ \nabla \cdot \mathbf{v}^* &= 0 \end{aligned} \right\}, \quad (2.2)$$

where $\mathbf{v}^* = (u^*, w^*)$ is the velocity, p^* is the perturbation pressure, ρ_0^* is the reference density, g is gravity, α and β are the thermal expansion and haline contraction coefficients, k_T and k_S are the molecular diffusivities of temperature and salinity and ν is the molecular viscosity.

System (2.2) is non-dimensionalized using microstructure scales, on which direct effects of molecular dissipation play an essential role in system dynamics. In particular, $d = (k_T \nu / g \alpha |A_T|)^{1/4}$, k_T/d , d^2/k_T and $\rho_0^* \nu k_T / d^2$ represent the units of length, velocity, time and pressure respectively (e.g. Radko 2013). The expansion/contraction coefficients (α , β) are incorporated in (T^*, S^*) , and $\alpha |A_T| d$ is used as the scale for both temperature and salinity perturbations

$$\alpha T^* \rightarrow \alpha |A_T| dT, \quad \beta S^* \rightarrow \alpha |A_T| dS. \tag{2.3a,b}$$

After non-dimensionalization, the governing equations reduce to

$$\left. \begin{aligned} \frac{\partial T}{\partial t} + \mathbf{v} \cdot \nabla T + s w &= \nabla^2 T \\ \frac{\partial S}{\partial t} + \mathbf{v} \cdot \nabla S + s \frac{w}{R_\rho} &= \tau \nabla^2 S \\ \frac{\partial}{\partial t} \mathbf{v} + \mathbf{v} \cdot \nabla \mathbf{v} &= Pr [-\nabla p + (T - S) \mathbf{k} + \nabla^2 \mathbf{v}] \\ \nabla \cdot \mathbf{v} &= 0 \end{aligned} \right\}, \tag{2.4}$$

where $R_\rho = \alpha A_T / \beta A_S$ is the background density ratio, $\tau = k_S / k_T$ is the diffusivity ratio, $Pr = \nu / k_T$ is the Prandtl number and $s = -1 (s = 1)$ for the diffusive (fingering) stratification.

The governing system (2.4) is further simplified using the vorticity–streamfunction formulation

$$\left. \begin{aligned} \frac{\partial T}{\partial t} + J(\psi, T) + s \frac{\partial \psi}{\partial x} &= \nabla^2 T \\ \frac{\partial S}{\partial t} + J(\psi, S) + \frac{s}{R_\rho} \frac{\partial \psi}{\partial x} &= \tau \nabla^2 S \\ \frac{\partial}{\partial t} \nabla^2 \psi + J(\psi, \nabla^2 \psi) &= Pr \left[\frac{\partial}{\partial x} (T - S) + \nabla^4 \psi \right] \end{aligned} \right\}, \tag{2.5}$$

where ψ is the streamfunction, such that $(u, w) = (-\partial \psi / \partial z, \partial \psi / \partial x)$, and $J(a, b) \equiv (\partial a / \partial x)(\partial b / \partial z) - (\partial a / \partial z)(\partial b / \partial x)$ is the Jacobian. The conversion between dimensional and non-dimensional units is based on the following nominal values of governing parameters:

$$\begin{aligned} \rho_0^* \sim 10^3 \text{ kg m}^{-3}, \quad g \sim 10 \text{ m s}^{-2}, \quad \nu \sim 10^{-6} \text{ m}^2 \text{ s}^{-1}, \quad k_T \sim 10^{-7} \text{ m}^2 \text{ s}^{-1}, \\ k_S \sim 10^{-9} \text{ m}^2 \text{ s}^{-1}, \quad \alpha \sim 10^{-4} \text{ K}^{-1}, \quad |A_T| \sim 0.01 \text{ K m}^{-1}, \end{aligned} \tag{2.6}$$

which suggest $d = 0.01$ m, $Pr = 10$ and $\tau = 0.01$.

The present investigation is focused on analytical and numerical solutions of governing equations (2.5) representing the evolution of large-scale internal waves in thermohaline staircases. Simulations are performed using a parallel dealiased spectral model (e.g. Stellmach *et al.* 2011; Radko 2019b) with periodic boundary conditions for (T, S, \mathbf{v}) . The DNS representing wave/staircase interactions are computationally expensive. The key complication is imposed by the requirement to resolve a wide range of dynamically significant scales – from the dimensions of an internal wave (L_x, L_z) , which we assume

greatly exceed the staircase step height ($h \ll L_z$), to the heat dissipation scale ($d \ll h$) and, finally, to the salinity dissipation scale ($d_s \sim \sqrt{\tau}d \ll d$). At present, DNS that can capture wave/staircase interactions for typical oceanic parameters can only be performed in two dimensions. Nevertheless, two-dimensional (2-D) models in double-diffusive convection are known to be generally consistent with their 3-D counterparts (e.g. Flanagan *et al.* 2013; Radko *et al.* 2015) and therefore our study is expected to adequately represent the system dynamics.

3. Preliminary simulations

To glean some insight into the basics of wave/staircase interaction, we first examine the DNS of a diffusive ($s = -1$) system in figures 1–3. This experiment consists of two distinct phases. The first (spin-up) phase (figure 1) was initiated by introducing a set of $n = 8$ horizontal layers at rest with homogeneous total temperature and salinity values (T_{tot}, S_{tot}) in each layer. Small-amplitude random noise was added to those fields to facilitate the development of active diffusive convection. The computational domain size in this experiment was $L_x \times L_z = 1600 \times 800$, which corresponds to 16 m \times 8 m for typical oceanographic conditions, and the numerical mesh contained $N_x \times N_z = 6144 \times 3072$ grid points. The choice of model parameters represents a compromise between the computational cost and our desire to model an effectively unbounded ocean. In studies of diffusive systems, it is common to characterize the background stratification using the inverse density ratio

$$R_\rho^{(inv)} \equiv \frac{1}{R_\rho} = \frac{\beta A_S}{\alpha A_T}, \tag{3.1}$$

and the simulation in figure 1 was performed with $R_\rho^{(inv)} = 3$, which is generally representative of Arctic staircases (e.g. Kelley *et al.* 2003; Timmermans *et al.* 2008). The dimensional buoyancy frequency in this case is

$$N^* \equiv \sqrt{-\frac{g}{\rho_0^*} \frac{\partial \rho_{bg}}{\partial z^*}} = \sqrt{g(\beta A_S - \alpha A_T)} = \sqrt{g\alpha(R_\rho^{(inv)} - 1)|A_T|} = 4.5 \cdot 10^{-3} \text{ s}^{-1}, \tag{3.2}$$

and its non-dimensional counterpart reduces to $N = \sqrt{(R_\rho^{(inv)} - 1)Pr} = 4.5$.

Shortly after initiation (figure 1a), the system starts its transition to fully developed diffusive convection, which is manifested first by the formation of diffusive plumes emanating from the interfaces between homogeneous layers (figure 1b). The growth and vertical spreading of diffusive plumes is followed by the establishment of a quasi-steady circulation pattern, characterized by active convective overturns in layers (figure 1c). To ensure that the system reaches statistical equilibrium by the end of the spin-up phase, each simulation of this nature was extended for at least 200 units of time, which is dimensionally equivalent to approximately 60 hours.

To explore the interaction of fully developed staircases with internal waves, the second stage of the experiment was initiated by introducing into the system a large-scale wave

$$\left. \begin{aligned} T_w &= \hat{T}_w \cos(kx + mz), \\ S_w &= \hat{S}_w \cos(kx + mz), \quad \hat{S}_w = R_\rho^{(inv)} \hat{T}_w, \\ \psi_w &= \hat{\psi}_w \cos(kx + mz), \quad \hat{\psi}_w = -\sqrt{Pr \frac{R_\rho^{(inv)} - 1}{k^2 + m^2}} \hat{T}_w. \end{aligned} \right\} \tag{3.3}$$

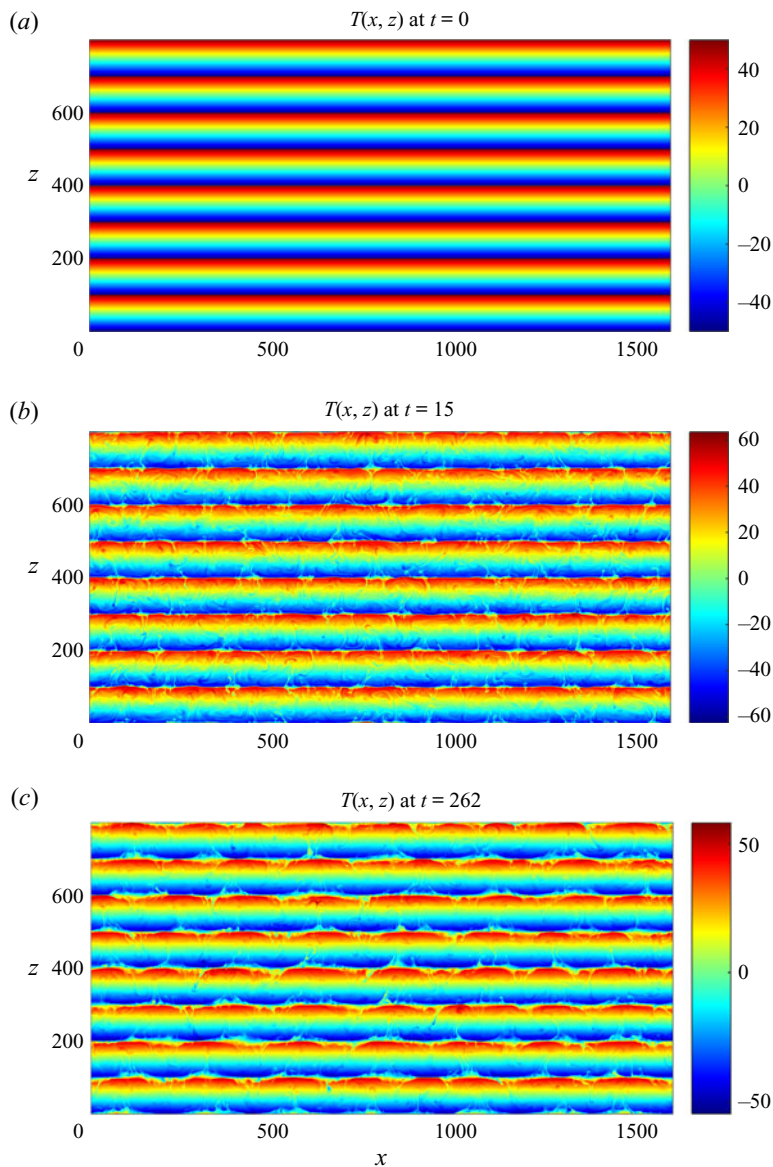


FIGURE 1. The spin-up phase of the diffusive DNS. The instantaneous temperature anomaly fields are shown at various times in (a–c). The experimental parameters are: $h = 100$, $R_\rho^{(inv)} = 3$, $\tau = 0.01$, $Pr = 10$, $L_x = 1600$, $L_z = 800$, $N_x = 6144$ and $N_z = 3072$.

The x - and z -wavelengths of this pattern match the size of the computational domain

$$\frac{2\pi}{k} = L_x, \quad \frac{2\pi}{m} = L_z, \quad (3.4a,b)$$

and therefore (3.3) conforms to the periodic boundary conditions assumed by the model. In the absence of other perturbations and dissipative effects, (3.3) would represent a free ideal wave oscillating at frequency $\omega = k\sqrt{Pr((R_\rho^{(inv)} - 1)/(k^2 + m^2))}$.

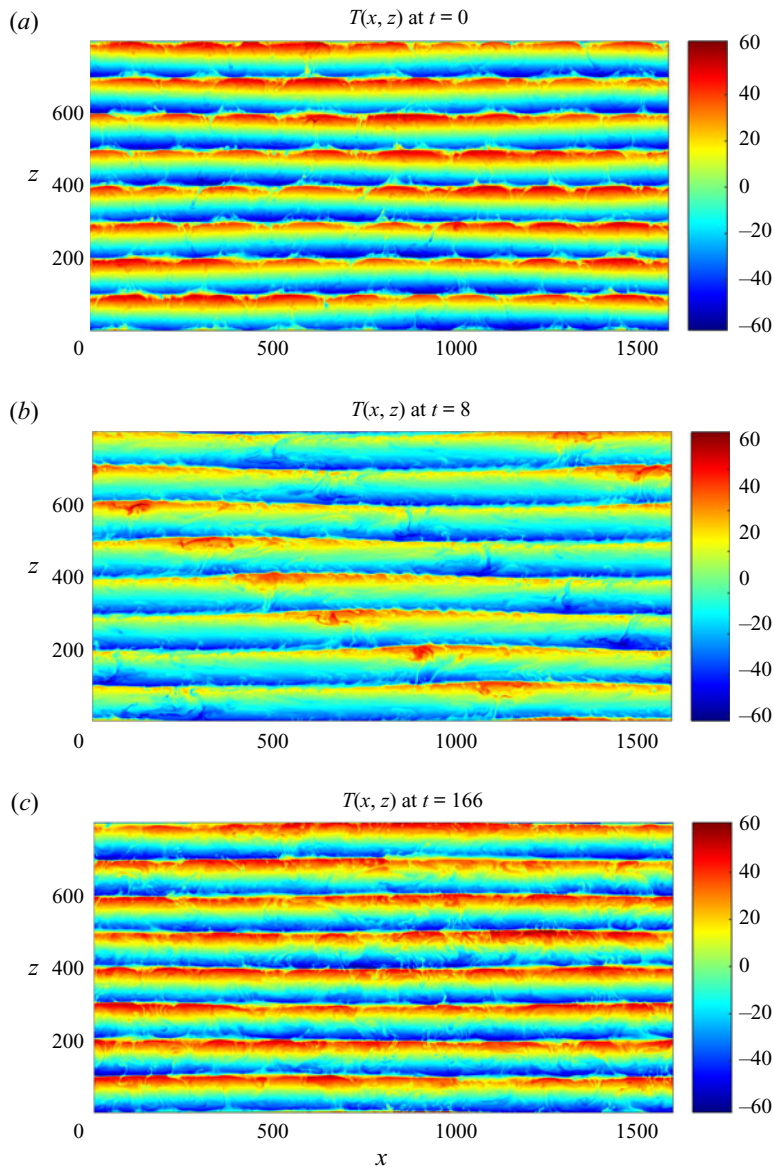


FIGURE 2. The second phase of the diffusive DNS. The internal wave (3.3) with the amplitude of $\hat{T}_w = 0.01L_z$ is superimposed on the fully developed state in figure 1(c). The instantaneous temperature anomaly fields are shown at various times in (a–c).

The wave pattern (3.3) with a relatively low amplitude of $\hat{T}_w = 0.01L_z$ was instantaneously superimposed on the state in figure 1(c) and the evolution of the resulting system is illustrated in figure 2. Adding the internal wave results in the visible distortion of the staircase (figure 2a), manifested most clearly in the periodic displacement of its interfaces. This large-scale perturbation systematically weakens in time (figure 2b) and largely disappears by $t = 166$ after the initiation of the second stage (figure 2c). To quantify the observed damping, we compute the net perturbation energy contained in the (k, m) harmonic as a function of time. In non-dimensional units, this quantity takes the following form:

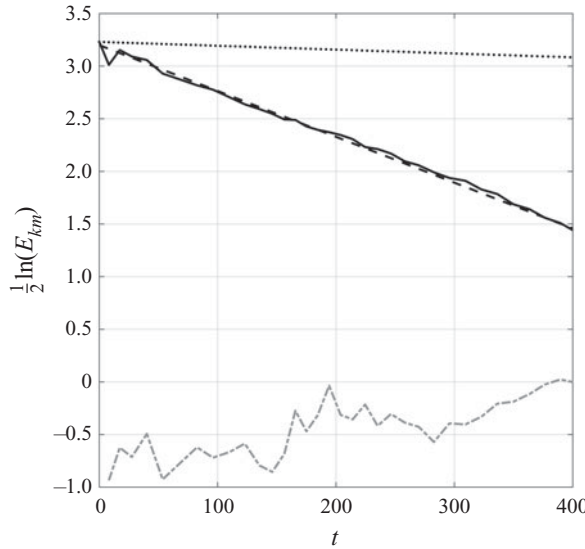


FIGURE 3. The solid curve represents the temporal record of $\frac{1}{2} \ln(E_{km})$ for the simulation in figure 2, where E_{km} is the perturbation energy contained in the mode (k, m) . The best linear fit for this record is indicated by the dashed line. The dotted line represents the corresponding pattern for the experiment without the staircase, in which the wave decay is less rapid. Also shown (the dash-dot grey curve) is the corresponding time series for the reflected wave $(k, -m)$.

$$E_{km} = \frac{1}{4} \left(Pr \frac{\hat{\rho}_c^2 + \hat{\rho}_s^2}{R_\rho^{(inv)} - 1} + \hat{u}_c^2 + \hat{u}_s^2 + \hat{w}_c^2 + \hat{w}_s^2 \right), \tag{3.5}$$

where $\hat{u}_{c,s}$, $\hat{w}_{c,s}$ and $\hat{\rho}_{c,s}$ represent the amplitudes of the velocity components and density. These amplitudes are evaluated for every output of field variables (u, w, T, S) as follows:

$$\left. \begin{aligned} \hat{u}_c &= 2[u \cos(kx + mz)]_{xz}, & \hat{u}_s &= 2[u \sin(kx + mz)]_{xz}, \\ \hat{w}_c &= 2[w \cos(kx + mz)]_{xz}, & \hat{w}_s &= 2[w \sin(kx + mz)]_{xz}, \\ \hat{\rho}_c &= 2[(S - T) \cos(kx + mz)]_{xz}, & \hat{\rho}_s &= 2[(S - T) \sin(kx + mz)]_{xz}, \end{aligned} \right\} \tag{3.6}$$

where symbol $[\dots]_{xz}$ denotes the spatial averaging. Using (3.5) and (3.6), the energy was evaluated and recorded for the experiment in figure 2 and $\frac{1}{2} \ln(E_{km})$ is plotted as a function of time in figure 3. This plot reveals that, after the initial adjustment period, the internal wave energy starts to decay in an approximately exponential manner. The decay rate (λ_d) was computed from the best linear fit to the time record of $\frac{1}{2} \ln(E_{km})$, which yielded

$$\lambda_d = 4.35 \cdot 10^{-3}, \tag{3.7}$$

with the 95 % confidence interval of $\Delta\lambda_{ci} = 1.91 \cdot 10^{-4}$. The corresponding e -folding decay time scale (λ_d^{-1}) is equivalent to 73 wave periods ($2\pi/\omega$), which indicates that the wave interaction with the staircase is relatively weak. This property is exploited in the following asymptotic model (§4), which analyses the staircase-induced modification of the ideal wave solution. For representative oceanic parameters (2.6), the dimensional e -folding decay time scale amounts to approximately two days. To confirm that the wave attenuation is caused by its interaction with the staircase, the experiment in figure 2 was

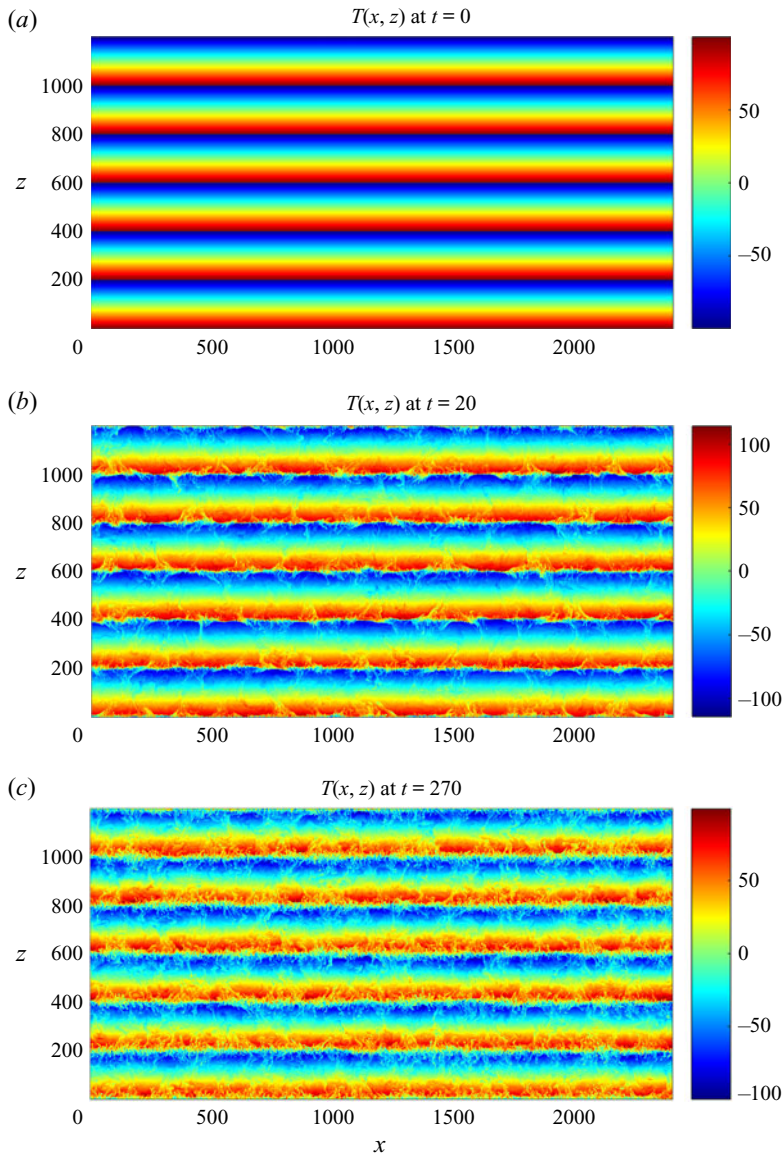


FIGURE 4. The spin-up phase of the fingering DNS. The instantaneous temperature anomaly fields are shown at various times in (a–c). The experimental parameters are: $h = 200$, $R_\rho = 1.5$, $\tau = 0.1$, $Pr = 10$, $Pr = 10$, $L_x = 2400$, $L_z = 1200$, $N_x = 6144$ and $N_z = 3072$.

reproduced using (3.3) as the initial condition with no staircase present. This simulation, which is also shown in figure 3, resulted in the decay rate of

$$\lambda_d = 3.66852 \cdot 10^{-4}, \tag{3.8}$$

with the 95 % confidence interval of $\Delta\lambda_{ci} = 1.75 \cdot 10^{-7}$. Thus, the wave decay rate in a uniform stratification is an order of magnitude less than in the staircase. In figure 3, we also present the corresponding energy record for the reflected mode with wavenumbers $(k, -m)$. These diagnostics are inspired by a recent model of internal waves incident upon a staircase from remote sources (Sutherland 2016). Sutherland’s theory attributes the

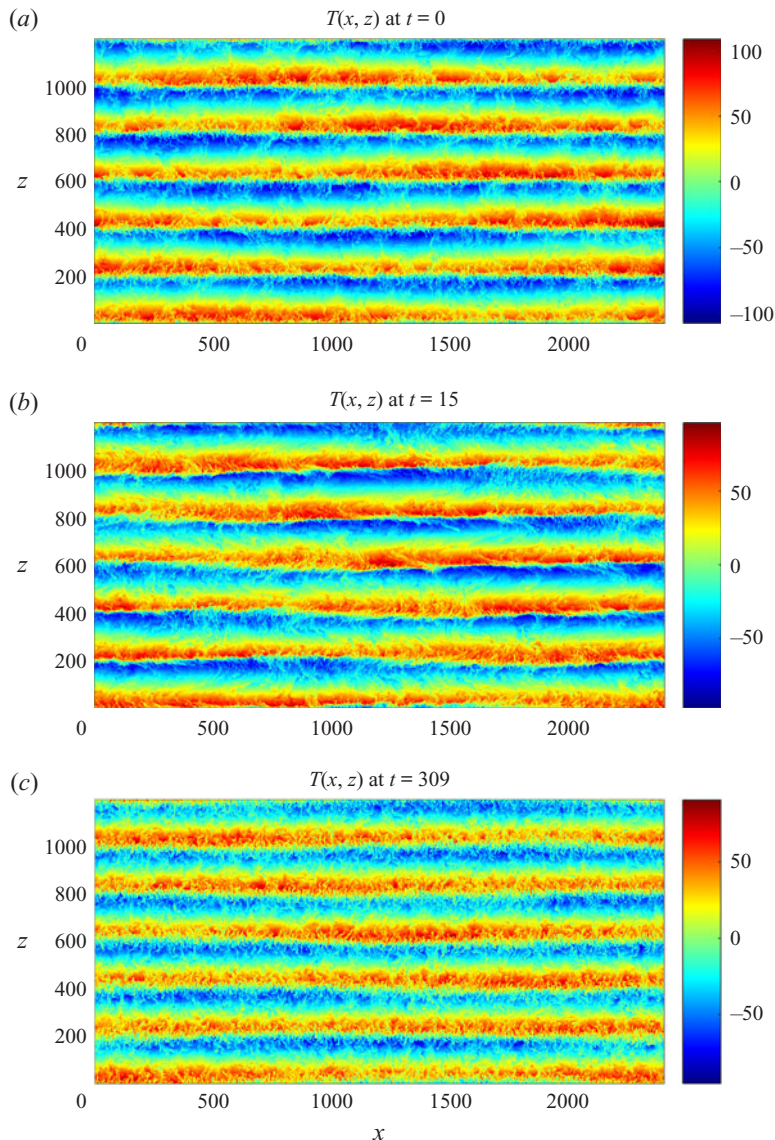


FIGURE 5. The second phase of the diffusive DNS. The internal wave with the amplitude of $\hat{T}_w = 0.01L_z$ is superimposed on the fully developed state in figure 4(c). The instantaneous temperature anomaly fields are shown at various times in (a–c).

adverse action of the staircase to the reflection of waves from high-gradient interfaces, prompting the question of whether the analogous dynamics is realized in the present system. The results in figure 3 indicate that wave reflection does not play a significant role in our simulations. In the course of the experiment in figure 3, the net energy loss by the primary mode (k, m) exceeds the energy gain by the reflected wave $(k, -m)$ by a factor of 430. This finding motivates the search for alternative mechanisms of suppression, which will be identified using the multiscale model in §§ 4 and 5.

Figures 4–6 present the corresponding calculation performed in the fingering regime ($s = 1$). This configuration presents a major computational challenge even in two

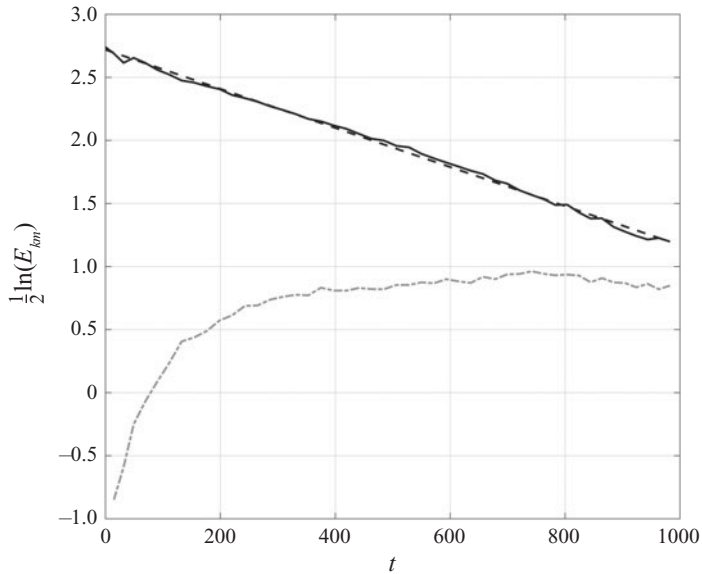


FIGURE 6. The solid curve represents the temporal record of $\frac{1}{2} \ln(E_{km})$ for the simulation in figure 5, where E_{km} is the perturbation energy contained in the mode (k, m) . The best linear fit for this pattern is indicated by the dashed line. The dash-dot grey curve represents the corresponding time series for the reflected wave $(k, -m)$.

dimensions since structurally stable fingering staircases are only realized for sufficiently large step heights $h \gtrsim 200$ (Radko 2014). Fingering simulations are generally more energetic, and therefore the salinity dissipation scale tends to be less than in the corresponding diffusive DNS. Therefore, the fingering experiment in figures 4–6 was performed with the dissipation ratio of $\tau = 0.1$, which is higher than realized in the ocean ($\tau \sim 0.01$) but still small. Fortunately, the actual value of the diffusivity ratio has a limited influence on fingering dynamics and intensity as long as it is significantly less than unity (e.g. Stern *et al.* 2001; Radko 2008). The step height in the following simulation is $h = 200$, the computational domain size is $L_x \times L_z = 2400 \times 1200$, the number of layers is $n = 6$ and the mesh contains $N_x \times N_z = 6144 \times 3072$ grid points.

The spin-up phase (figure 4) was effectively completed by $t = 200$, resulting in a quasi-equilibrium state (figure 4c). Note that the interfaces realized in the fingering simulation are not as sharp as their diffusive counterparts (cf. figure 1c) but the layered pattern of the staircase is still well defined. Figure 5 illustrates the decay of the wave with the amplitude of $\hat{T}_w = 0.01L_z$ that was added to the state in figure 4(c). The perturbation systematically weakens in time (cf. figure 5a–c). It is barely visible in the temperature field shown in figure 5(c), which was recorded at $t = 309$. Figure 6 presents the temporal record of $\frac{1}{2} \ln(E_{km})$ along with its best linear fit, from which the decay rate was determined to be $\lambda_d = 1.55 \cdot 10^{-3}$. This rate is comparable but less than the corresponding value for the diffusive case (figure 3). The reflected harmonic $(k, -m)$ in the fingering simulation is more pronounced than in the diffusive case. Still, the net loss of energy by the primary wave in figure 6 substantially (by a factor of 43) exceeds the energy gain by the reflected wave, which argues against the significant contribution of reflection to wave suppression. To fully explain the dynamics of wave–staircase interaction and efficiently explore the parameter space, we now turn to an asymptotic multiscale model.

4. Multiscale theory

4.1. Model development

The evolution of large-scale internal waves in the staircase is described using the new set of variables (X, Z, t_2) that are related to the original ones through

$$(X, Z) = \varepsilon(x, z), \quad t_2 = \varepsilon^2 t, \tag{4.1a,b}$$

where $\varepsilon \ll 1$ is the scale-separation parameter. Variables (x, z, t) are used to describe the processes that operate on the scale of staircase steps (h), whereas (X, Z, t_2) represent the dynamics on the scale of internal waves. To be specific, the small parameter is defined as the ratio of step height and the vertical wavelength of the internal wave

$$\varepsilon = \frac{h}{L_z}. \tag{4.2}$$

The basic state in the following model consists of z -periodic and x -independent temperature and salinity patterns $\bar{T}(z)$ and $\bar{S}(z)$ representing the layered step-like diffusive ($s = -1$) stratification.

The assumed x -invariance of staircase properties represents a significant idealization, which lacks some attributes of observed structures, such as convective overturns in mixed layers and double-diffusive microstructure within the interfaces. The small-scale x -dependent patterns are clearly visible in DNS, both diffusive (e.g. figures 1 and 2) and fingering (e.g. figures 4 and 5). Nevertheless, we believe that such an approach can offer a deeper insight into the wave–staircase interaction problem. Aside from the obvious advantages of simplicity and dynamical transparency, it also affords an opportunity to compare predictions of the reduced-dynamics model with more general DNS-based calculations. The differences and similarities in the results will inform us about the relative significance of the processes neglected by the idealized model.

Given the x -invariance of the basic patterns and the absence of any small-scale variability in the primary wave, their interaction is expected to generate secondary patters that are also devoid of small-scale variability in x . Hence, it becomes unnecessary to use the small-scale horizontal variable in the following analysis. The spatial and time derivatives in governing equations (2.4) are therefore replaced as follows:

$$\frac{\partial}{\partial x} \rightarrow \varepsilon \frac{\partial}{\partial X}, \quad \frac{\partial}{\partial z} \rightarrow \frac{\partial}{\partial z} + \varepsilon \frac{\partial}{\partial Z}, \quad \frac{\partial}{\partial t} \rightarrow \frac{\partial}{\partial t} + \varepsilon^2 \frac{\partial}{\partial t_2}, \tag{4.3a-c}$$

and both sets of variables are treated as independent variables.

Using (4.3a-c), governing equations (2.5) are expressed in terms of both small-scale and large-scale variables, resulting in

$$\left. \begin{aligned} \frac{\partial T}{\partial t} + \varepsilon^2 \frac{\partial T}{\partial t_2} + \varepsilon J_{Xz}(\psi, T) + \varepsilon^2 J_{XZ}(\psi, T) - \varepsilon \frac{\partial \psi}{\partial X} &= \nabla^2(T - \bar{T}) \\ \frac{\partial S}{\partial t} + \varepsilon^2 \frac{\partial S}{\partial t_2} + \varepsilon J_{Xz}(\psi, S) + \varepsilon^2 J_{XZ}(\psi, S) - \varepsilon R_\rho^{(inv)} \frac{\partial \psi}{\partial X} &= \tau \nabla^2(S - \bar{S}) \\ \frac{\partial \zeta}{\partial t} + \varepsilon^2 \frac{\partial \zeta}{\partial t_2} + \varepsilon J_{Xz}(\psi, \zeta) + \varepsilon^2 J_{XZ}(\psi, \zeta) &= Pr \left[\varepsilon \frac{\partial}{\partial X}(T - S) + \nabla^2 \zeta \right] \\ \zeta = \nabla^2 \psi, \quad \nabla^2 \equiv \varepsilon^2 \frac{\partial^2}{\partial X^2} + \frac{\partial^2}{\partial z^2} + 2\varepsilon \frac{\partial^2}{\partial z \partial Z} + \varepsilon^2 \frac{\partial^2}{\partial Z^2} \end{aligned} \right\}, \tag{4.4}$$

where $J_{XZ}(a, b) \equiv (\partial a/\partial X)(\partial b/\partial Z) - (\partial a/\partial Z)(\partial b/\partial X)$ and $J_{Xz}(a, b) \equiv (\partial a/\partial X)(\partial b/\partial z) - (\partial a/\partial z)(\partial b/\partial X)$ are the Jacobians in (X, Z) and (X, z) respectively. To ensure that (\bar{T}, \bar{S}) represent the steady state, the temperature and salinity equations in (4.4) are augmented by introducing forcing terms $(-\nabla^2 \bar{T}, -\tau \nabla^2 \bar{S})$. These terms prevent diffusive dissipation of the basic state, thereby representing the action of microscale processes maintaining thermohaline staircases in the ocean.

To analyse the interaction between waves and the staircase, we seek the solution of governing equations in terms of power series in $\varepsilon \ll 1$ as follows:

$$\left. \begin{aligned} T &= \bar{T}(z) + \varepsilon T_1(X, z, Z, t, t_2) + \varepsilon^2 T_2(X, z, Z, t, t_2) + \dots \\ S &= \bar{S}(z) + \varepsilon S_1(X, z, Z, t, t_2) + \varepsilon^2 S_2(X, z, Z, t, t_2) + \dots \\ \psi &= \psi_w(X, Z, t, t_2) + \varepsilon \psi_1(X, z, Z, t, t_2) + \varepsilon^2 \psi_2(X, z, Z, t, t_2) + \dots \end{aligned} \right\}, \quad (4.5)$$

where ψ_w is the leading-order streamfunction component of a large-scale internal wave. We assume the harmonic form for ψ_w

$$\psi_w = \hat{\psi}_w \exp\{i(KX + MZ - \omega_0 t - \omega_2 t_2)\}, \quad (4.6)$$

where $(K, M) = \varepsilon^{-1}(k, m)$ are the large-scale wavenumbers. The zero-order frequency is denoted by ω_0 , and ω_2 is the correction associated with the variation on the slow time scale. The imaginary component of the perturbation frequency measures the rate of wave decay

$$\lambda_d = -\text{Im}(\omega) = -\text{Im}(\omega_0) - \varepsilon^2 \text{Im}(\omega_2). \quad (4.7)$$

We substitute (4.5) and (4.6) in governing equations (4.4) and sequentially solve the hierarchy of balances realized at each order in ε until an explicit expression for ω_2 is found. At each order, we retain only terms that are linear in the wave amplitude ($\hat{\psi}_w$). This linearization with respect to $\hat{\psi}_w$ makes it possible to unambiguously determine the linear decay rate of the primary wave, which is one of the principal objectives of the following analysis.

The $O(1)$ balances of (4.4) are trivially satisfied by the combination of primary wave and the staircase. The $O(\varepsilon)$ balances of T - S equations require that

$$\left. \begin{aligned} T_1 &= (\hat{T}_w + \hat{\psi}_w \tilde{T}_1(z)) \exp\{i(KX + MZ - \omega_0 t - \omega_2 t_2)\} \\ S_1 &= (\hat{S}_w + \hat{\psi}_w \tilde{S}_1(z)) \exp\{i(KX + MZ - \omega_0 t - \omega_2 t_2)\} \end{aligned} \right\}, \quad (4.8)$$

where $\hat{T}_w = -K\hat{\psi}_w/\omega_0$ and $\hat{S}_w = -KR_\rho^{(inv)}\hat{\psi}_w/\omega_0$. The coefficients (\hat{T}_w, \hat{S}_w) represent the amplitudes of temperature and salinity fields in the primary large-scale wave. However, the nonlinear interaction of the primary wave with the small-scale staircase – the interaction represented by terms $J_{Xz}(\psi, T)$ and $J_{Xz}(\psi, S)$ in (4.4) – also produces small-scale $O(\varepsilon)$ components of temperature and salinity. This dynamics is accounted for by the inclusion of auxiliary functions $(\tilde{T}_1, \tilde{S}_1)$ in (4.8), which satisfy ordinary differential equations

$$\left. \begin{aligned} iK \frac{d\tilde{T}}{dz} - i\omega_0 \tilde{T}_1 - \frac{d^2 \tilde{T}_1}{dz^2} &= 0 \\ iK \frac{d\tilde{S}}{dz} - i\omega_0 \tilde{S}_1 - \tau \frac{d^2 \tilde{S}_1}{dz^2} &= 0 \end{aligned} \right\}. \quad (4.9)$$

A unique solution for auxiliary functions arising at each order in the expansion is determined by requiring their mean value in z to be zero. These functions are represented by complex numbers and their arguments measure the phase shifts of the corresponding flow components relative to the primary large-scale wave ψ_w . Note that, unlike T - S equations, the vorticity equation at $O(\varepsilon)$ does not reflect the interaction between primary wave and the basic staircase pattern, and therefore we set $\psi_1 = 0$.

The $O(\varepsilon^2)$ balances are solved using

$$\left. \begin{aligned} T_2 &= \hat{\psi}_w \tilde{T}_2(z) \exp\{i(KX + MZ - \omega_0 t - \omega_2 t_2)\} \\ S_2 &= \hat{\psi}_w \tilde{S}_2(z) \exp\{i(KX + MZ - \omega_0 t - \omega_2 t_2)\} \\ \psi_2 &= \hat{\psi}_w (\tilde{\psi}_{2w} + \tilde{\psi}_2(z)) \exp\{i(KX + MZ - \omega_0 t - \omega_2 t_2)\} \end{aligned} \right\}, \tag{4.10}$$

where $(\tilde{T}_2, \tilde{S}_2, \tilde{\psi}_2)$ satisfy

$$\left. \begin{aligned} 2iM \frac{d\tilde{T}_1}{dz} + i\omega_0 \tilde{T}_2 + \frac{d^2 \tilde{T}_2}{dz^2} &= 0 \\ 2iM\tau \frac{d\tilde{S}_1}{dz} + i\omega_0 \tilde{S}_2 + \tau \frac{d^2 \tilde{S}_2}{dz^2} &= 0 \\ -iPr \frac{d^4 \tilde{\psi}_2}{dz^4} + \omega_0 \frac{d^2 \tilde{\psi}_2}{dz^2} - KPr(\tilde{S}_1 - \tilde{T}_1) &= 0 \end{aligned} \right\}. \tag{4.11}$$

The solvability condition that arises at this order requires that

$$\omega_0^2 = \frac{K^2(R_\rho^{(inv)} - 1)Pr}{K^2 + M^2}. \tag{4.12}$$

In (4.12), we readily recognize the dispersion relation of free non-dissipative internal waves in the linear background gradient, written here in the non-dimensional form. This is an expected result since (4.6) represents is an internal wave with dimensions greatly exceeding the staircase step height. Neither molecular dissipation nor the presence of a staircase influences the evolution of this primary wave at the leading order. Equation (4.12) also implies that $\text{Im}(\omega_0) = 0$ and the wave decay (4.7) reduces to

$$\lambda_d = -\varepsilon^2 \text{Im}(\omega_2). \tag{4.13}$$

The essential dynamics of staircase-induced suppression is revealed by the third-order balances which imply that

$$\left. \begin{aligned} T_3 &= \hat{\psi}_w (\tilde{T}_{3w} + \tilde{T}_3(z)) \exp\{i(KX + MZ - \omega_0 t - \omega_2 t_2)\} \\ S_3 &= \hat{\psi}_w (\tilde{S}_{3w} + \tilde{S}_3(z)) \exp\{i(KX + MZ - \omega_0 t - \omega_2 t_2)\} \\ \psi_3 &= \hat{\psi}_w \tilde{\psi}_3(z) \exp\{i(KX + MZ - \omega_0 t - \omega_2 t_2)\} \end{aligned} \right\}, \tag{4.14}$$

where

$$\left. \begin{aligned}
 & i\omega_0 K(\tilde{\psi}_{2w} + \tilde{\psi}_2) \left(\frac{d\tilde{T}}{dz} - 1 \right) - \frac{d^2\tilde{T}_3}{dz^2} \omega_0 - 2iM\omega_0 \frac{d\tilde{T}_2}{dz} + (K^2 + M^2 - i\omega_2)\omega_0\tilde{T}_1 \\
 & \quad + iK\omega_2 - i\tilde{T}_3\omega_0^2 - i\tilde{T}_{w3}\omega_0^2 - K^3 - KM^2 = 0 \\
 & i\omega_0 K(\tilde{\psi}_{2w} + \tilde{\psi}_2) \left(\frac{d\tilde{S}}{dz} - R_\rho^{(inv)} \right) - \frac{d^2\tilde{S}_3}{dz^2} \omega_0\tau - 2iM\omega_0 \frac{d\tilde{S}_2}{dz} \tau + (K^2\tau + M^2\tau - i\omega_2)\omega_0\tilde{S}_1 \\
 & \quad + iK\omega_2 R_\rho^{(inv)} - i\tilde{S}_3\omega_0^2 - i\hat{S}_{3w}\omega_0^2 - K^3 R_\rho^{(inv)} \tau - KM^2 R_\rho^{(inv)} \tau = 0 \\
 & Pr \frac{d^4\tilde{\psi}_3}{dz^4} + 4iM Pr \frac{d^3\tilde{\psi}_3}{dz^3} + i \frac{d^2\tilde{\psi}_3}{dz^2} \omega_0 - 2M \frac{d\tilde{\psi}_2}{dz} \omega_0 - iK Pr(\tilde{S}_2 - \tilde{T}_2) = 0
 \end{aligned} \right\} \quad (4.15)$$

The emergence of the secondary large-scale plane-wave harmonic with the amplitude $(\varepsilon^3\tilde{T}_{3w}, \varepsilon^3\tilde{S}_{3w}, \varepsilon^2\tilde{\psi}_{2w})\hat{\psi}_w$ is triggered by the nonlinear interaction between the second-order wave-induced perturbation in the streamfunction and the basic staircase pattern. These interactions are reflected by terms $i\omega_0 K\tilde{\psi}_2(d\tilde{T}/dz)$ and $i\omega_0 K\tilde{\psi}_2(d\tilde{S}/dz)$ in temperature and salinity equations of (4.15). Importantly, no analogous nonlinear terms arise in the vorticity equation at this order. Since $\tilde{\psi}_2$ is not necessarily orthogonal to the basic state, their interaction produces patterns varying on large scales (X, Z) . This dynamics is brought to the fore by z -averaging the temperature and salinity equations in (4.15) and solving the resulting equations for $(\tilde{T}_{3w}, \tilde{S}_{3w})$

$$\left. \begin{aligned}
 \tilde{T}_{3w} &= iK\omega_0^{-2}(i\tilde{\psi}_{2w}\omega_0 - iN_T\omega_0 + K^2 + M^2 - i\omega_2) \\
 \tilde{S}_{3w} &= iK\omega_0^{-2}(i\tilde{\psi}_{2w}\omega_0 R_\rho^{(inv)} - iN_S\omega_0 + K^2 R_\rho^{(inv)} + M^2 R_\rho^{(inv)} - i\omega_2 R_\rho^{(inv)})
 \end{aligned} \right\}, \quad (4.16)$$

where (N_T, N_S) are the nonlinear terms

$$N_T = \left[\tilde{\psi}_2 \frac{d\tilde{T}}{dz} \right]_z, \quad N_S = \left[\tilde{\psi}_2 \frac{d\tilde{S}}{dz} \right]_z. \quad (4.17a,b)$$

These nonlinear terms, which will be shown to play a critical role in staircase-induced wave suppression, originate from the advective components $J_{Xz}(\psi, T)$ and $J_{Xz}(\psi, S)$ of the T - S equations in (4.4). They are readily interpreted as the result of large-scale vertical divergence of diapycnal eddy fluxes of heat and salt (F_T, F_S)

$$\left. \begin{aligned}
 iKN_T \exp\{i(KX + MZ - \omega_0 t - \omega_2 t_2)\} &= \frac{\partial}{\partial Z} F_T \\
 iKN_S \exp\{i(KX + MZ - \omega_0 t - \omega_2 t_2)\} &= \frac{\partial}{\partial Z} F_S
 \end{aligned} \right\}, \quad (4.18)$$

where

$$\left. \begin{aligned}
 \varepsilon^3 F_T &= l.o.\{[wT]_z\} \\
 \varepsilon^3 F_S &= l.o.\{[wS]_z\}
 \end{aligned} \right\}. \quad (4.19)$$

The notation $l.o.\{\dots\}$ in (4.19) is used to represent the leading-order component, which in this case is $O(\varepsilon^3)$. Note that the fluxes in (4.19) are averaged over small scales. This implies that the staircase-induced suppression is ultimately driven by eddy diffusion of temperature and salinity on the scale of staircase steps (h) . The analogous effects of eddy

viscosity do not appear at this order. The sought after expression for ω_2 is obtained as a solvability condition at $O(\varepsilon^4)$ as follows. The fourth-order balance of the vorticity equation yields

$$\begin{aligned}
 & -4iM \frac{\partial^3 \tilde{\psi}_3}{\partial z^3} Pr \omega_0^2 - \omega_0^2 (i\omega_2 + 2K^2 Pr - 6M^2 Pr) \frac{\partial^2 \tilde{\psi}_2}{\partial z^2} + 2 \frac{\partial \tilde{\psi}_3}{\partial z} M \omega_0^3 \\
 & - iK \tilde{T}_3 Pr \omega_0^2 + iK \tilde{S}_3 Pr \omega_0^2 \\
 & + i\omega_0^3 (K^2 + M^2) \tilde{\psi}_2 + (i\omega_2 - K^2 Pr - M^2 Pr) (K^2 + M^2) \omega_0^2 \\
 & - iPr K^2 (R_\rho^{(inv)} \tilde{\psi}_{w2} - \tilde{\psi}_{w2} - N_S + N_T) \omega_0 \\
 & + i\tilde{\psi}_{w2} (K^2 + M^2) \omega_0^3 + Pr K^2 ((1 - R_\rho^{(inv)} \tau) (K^2 + M^2) + i\omega_2 (R_\rho^{(inv)} - 1)) = 0. \tag{4.20}
 \end{aligned}$$

Equation (4.20) is greatly simplified by recognizing that the coefficient of $\tilde{\psi}_{w2}$ is exactly zero as long as ω_0 satisfies the dispersion relation (4.12). The resulting expression is then averaged in z , taking advantage of the periodicity of $\tilde{\psi}_2(z)$ and $\tilde{\psi}_3(z)$:

$$\begin{aligned}
 & (i\omega_2 - K^2 Pr - M^2 Pr) (K^2 + M^2) \omega_0^2 - iPr K^2 (N_T - N_S) \omega_0 \\
 & + Pr K^2 ((1 - R_\rho^{(inv)} \tau) (K^2 + M^2) + i\omega_2 (R_\rho^{(inv)} - 1)) = 0. \tag{4.21}
 \end{aligned}$$

Finally, (4.21) is solved for ω_2 and the result is further simplified using the dispersion relation (4.12)

$$\omega_2 = \frac{1}{2} \frac{(N_T - N_S) K \sqrt{Pr}}{\sqrt{(K^2 + M^2) (R_\rho^{(inv)} - 1)}} + \frac{i}{2} \frac{(K^2 + M^2) (Pr + 1 - (Pr + \tau) R_\rho^{(inv)})}{(R_\rho^{(inv)} - 1)}. \tag{4.22}$$

At this point, the multiscale analysis is completed, and we revert to the original variables using (4.1a,b). To simplify the transition, we denote $(\tilde{T}_{10}, \tilde{S}_{10}) = \varepsilon(\tilde{T}_1, \tilde{S}_1)$, $\tilde{\psi}_{20} = \varepsilon^2 \tilde{\psi}_2$, $N_{T0} = [\tilde{\psi}_{20} (d\tilde{T}/dz)]_z$, and $N_{S0} = [\tilde{\psi}_{20} (d\tilde{S}/dz)]_z$. As a result, the first-order balance (4.9) takes the form

$$\left. \begin{aligned}
 ik \frac{d\tilde{T}}{dz} - i\omega_0 \tilde{T}_{10} - \frac{d^2 \tilde{T}_{10}}{dz^2} &= 0 \\
 ik \frac{d\tilde{S}}{dz} - i\omega_0 \tilde{S}_{10} - \tau \frac{d^2 \tilde{S}_{10}}{dz^2} &= 0
 \end{aligned} \right\}, \tag{4.23}$$

and the second-order vorticity equation in (4.11) reduces to

$$-iPr \frac{d^4 \tilde{\psi}_{20}}{dz^4} + \omega_0 \frac{d^2 \tilde{\psi}_{20}}{dz^2} - kPr (\tilde{S}_{10} - \tilde{T}_{10}) = 0. \tag{4.24}$$

For any given periodic basic patterns (\tilde{T}, \tilde{S}) , (4.23) and (4.24) are solved for $(\tilde{T}_{10}, \tilde{S}_{10}, \tilde{\psi}_{20})$ using the Fourier transform in z . The decay rate can now be expressed in terms of the

original variables as follows:

$$\lambda_d = -\varepsilon^2 \text{Im}(\omega_2) = \text{Im} \left(\underbrace{\frac{1}{2} \frac{(N_{S0} - N_{T0})k\sqrt{Pr}}{\sqrt{(k^2 + m^2)(R_\rho^{(inv)} - 1)}}}_A \right) + \underbrace{\frac{1}{2} \frac{(k^2 + m^2)((Pr + \tau)R_\rho^{(inv)} - Pr - 1)}{(R_\rho^{(inv)} - 1)}}_B. \tag{4.25}$$

Equation (4.25) indicates that the weakening of the large-scale wave is controlled by two effects. Term *A* represents the wave interaction with the staircase – the dominant damping process and the subject of our study. Term *B*, on the other hand, represents the damping component that is realized even in the absence of the staircase. It is weak, driven entirely by the direct molecular dissipation of the large-scale wave, and can be neglected for most intents and purposes. The relative intensity of wave suppression in the staircase and the corresponding uniform gradient can be quantified using the diagnostic variable

$$r_d = \frac{A}{B}, \tag{4.26}$$

which will be referred to as the attenuation ratio. As a consistency check, term *B* can be readily evaluated for the parameters of the experiment in figure 3, which yields $B = 3.66833 \cdot 10^{-4}$. This value agrees with the DNS-based estimate of the decay rate in linear gradient (3.8) remarkably well, with the relative error of only $5.1 \cdot 10^{-5}$. Theory development for fingering staircases ($s = 1$) closely mimics the foregoing diffusive model, and the counterpart of (4.25) is

$$\lambda_d = \text{Im} \left(\frac{1}{2} \frac{(N_{S0} - N_{T0})k\sqrt{PrR_\rho}}{\sqrt{(k^2 + m^2)(R_\rho - 1)}} \right) + \frac{1}{2} \frac{(k^2 + m^2)((Pr + 1)R_\rho - Pr - \tau)}{(R_\rho - 1)}. \tag{4.27}$$

In the absence of planetary rotation, the expressions for the decay rate in both diffusive and fingering staircases can be readily obtained in three dimensions by replacing k in (4.25) and (4.27) by the total horizontal wavenumber $k_h = \sqrt{k^2 + \ell^2}$.

4.2. Interpretation

To trace and explain the sequence of processes resulting in the staircase-induced wave suppression, we now assume simple explicit patterns for (\bar{T}, \bar{S})

$$\left\{ \begin{array}{l} \bar{T} = \bar{T}_{tot} + z, \quad \bar{T}_{tot} = -\frac{h \tanh(\sin(\pi z/h)h_i^{-1})}{2 \tanh(h_i^{-1})} \\ \bar{S} = \bar{S}_{tot} + R_\rho^{(inv)}z, \quad \bar{S}_{tot} = -\frac{h}{2} R_\rho^{(inv)} \frac{\tanh(\sin(\pi z/h)h_i^{-1})}{\tanh(h_i^{-1})} \end{array} \right. \text{ for } -\frac{h}{2} < z < \frac{h}{2}. \tag{4.28}$$

Parameter h_i in (4.28) measures the thickness of high-gradient interfaces relative to the step height (h), and $h_i \sim 0.1$ is representative of oceanic staircases, both fingering and diffusive. The basic patterns (figure 7a,b) reflect the step-like structure of observed

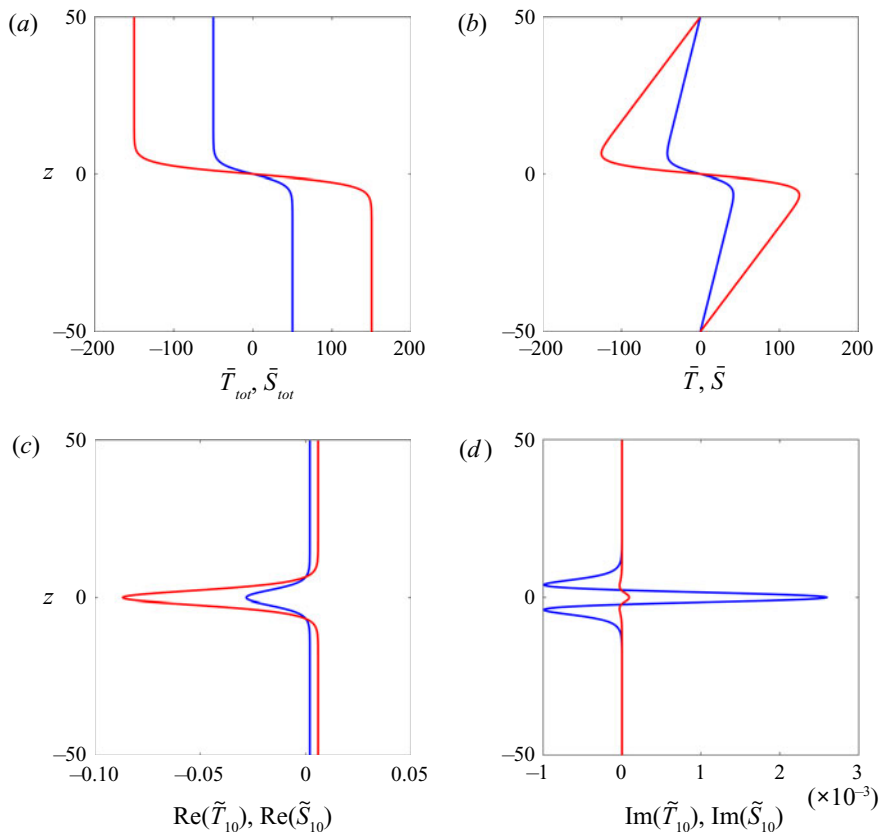


FIGURE 7. Multiscale model. The assumed total temperature and salinity fields in the unperturbed staircase are shown in (a). (b) shows the corresponding T - S anomalies. The real and imaginary components of the first-order T - S perturbations are shown in (c) and (d) respectively. The temperature (salinity) patterns are indicated by blue (red) curves. Model parameters match those used for the diffusive DNS in figures 1–3: $R_\rho^{(inv)} = 3$, $Pr = 10$, $\tau = 0.01$, $h = 100$, $h_i = 0.1$, $s = -1$.

staircases (e.g. Kelley *et al.* 2003). The specific choice (4.28) was motivated by our desire to construct an infinitely smooth profile that would satisfy periodic boundary conditions at $z = (-h/2, h/2)$ not only by (\bar{T}, \bar{S}) , but also by all their derivatives. However, additional calculations performed with $\tanh(az)$ and $\text{erf}(az)$ profiles indicate that the results obtained for the same interfacial thickness are largely insensitive to the profile choice.

The following calculation is performed for the parameters used in the foregoing diffusive DNS (figures 1–3). The immediate consequence of wave/staircase interaction is the tilting of high-gradient interfaces by the primary wave, which generates the first-order perturbation temperature and salinity fields $(\tilde{T}_{10}, \tilde{S}_{10})$. These functions, obtained by solving (4.23), are shown in figure 7(c,d). The T - S perturbations are localized in the vicinity of interfaces and their real components substantially exceed the imaginary ones. Neglecting $\text{Im}(\tilde{T}_{10})$ and $\text{Im}(\tilde{S}_{10})$ has no significant effect on the resulting solutions. This property implies that the first-order small-scale T - S perturbations lag the vertical wave velocity (w_w) by approximately a quarter phase, which is a fully expected kinematic consequence of vertical advection of temperature and salinity across high-gradient interfaces.

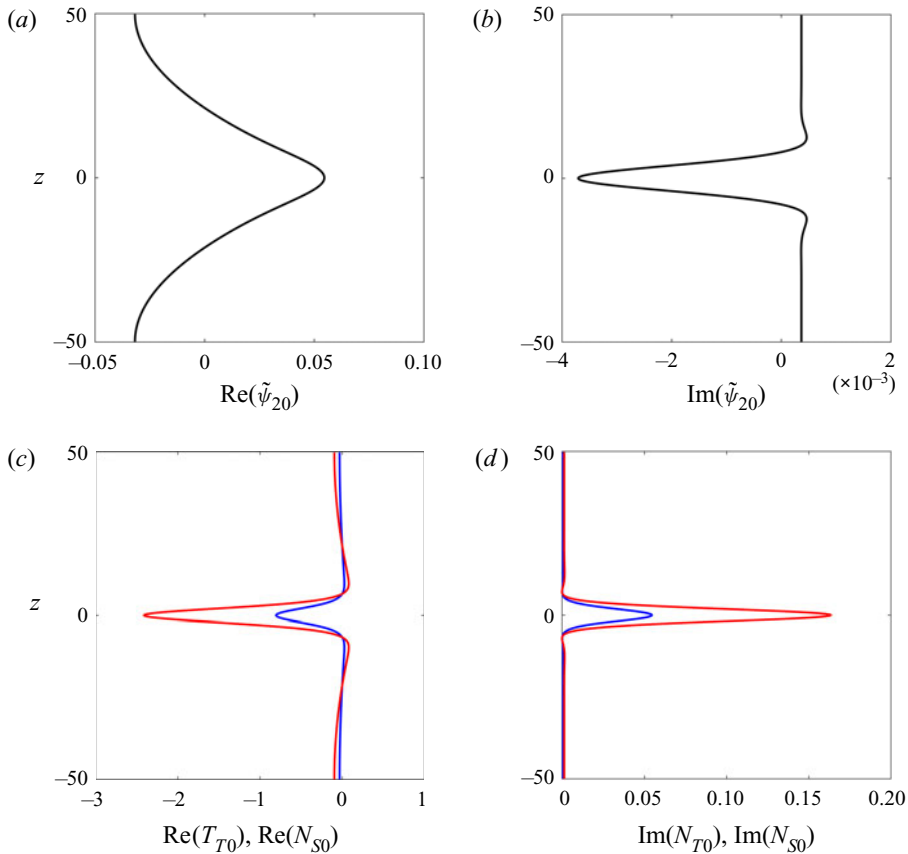


FIGURE 8. Multiscale model (figure 7). The real and imaginary components of the second-order streamfunction perturbation are shown in (a) and (b) respectively. The real and imaginary components of the nonlinear advective terms N_{T0} and N_{S0} are shown in (c) and (d) respectively. The temperature (salinity) advection terms N_{T0} (N_{S0}) are indicated by blue (red) curves.

The laterally non-uniform distribution of buoyancy associated with the first-order perturbation, in turn, induces the secondary circulation as lighter (denser) fluid at a given z -level tends to rise (sink). This secondary pattern is represented by $\text{Re}(\tilde{\psi}_{20})$ component in figure 8(a), which was determined by solving (4.24). On its own, this response can affect the frequency of the primary wave but does not lead to its systematic attenuation since it is in phase with the primary large-scale wave. The secondary circulation pattern, however, is also affected by viscous dissipation, represented by the term $-iPr(d^4\tilde{\psi}_{20}/dz^4)$ in the vorticity equation (4.24). Molecular friction generates a small (figure 8b) but dynamically essential correction $\text{Im}(\tilde{\psi}_{20})$. This circulation component opposes the flow pattern associated with $\text{Re}(\tilde{\psi}_{20})$ and lags it by a quarter of a period. The vertical velocities associated with $\text{Im}(\tilde{\psi}_{20})$ induce finite vertical advective fluxes of temperature and salinity ($-\bar{T}k \text{Im}(\tilde{\psi}_{20})$, $-\bar{S}k \text{Im}(\tilde{\psi}_{20})$). The resulting flux convergence patterns (figure 8d) oppose the T - S tendencies of the primary large-scale wave, causing its gradual dissipation.

The foregoing analysis implies that staircases play a catalytic role in damping large-scale waves. The interaction of the large-scale primary wave with the staircase produces new flow patterns that are localized in the vicinity of high-gradient interfaces. The advective

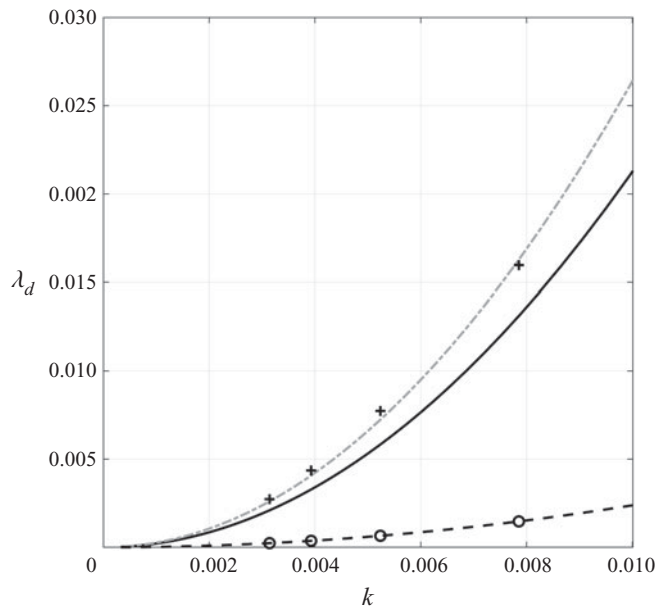


FIGURE 9. The wave decay rate (λ_d) in the diffusive staircase, evaluated using the multiscale theory for $h_i = 0.1$, is plotted as a function of its horizontal wavenumber (solid curve). The dash-dot grey curve represents the best fit of the theory and DNS, which is realized for $h_i = 0.0688$. The corresponding DNS-based values are indicated by the plus signs. The dashed curve shows the theoretical prediction of the decay rate in the absence of a staircase and the corresponding DNS results are indicated by circles.

fluxes of temperature and salinity associated with those patterns are more effective in damping the primary wave than molecular dissipation acting directly on the primary large-scale wave. At the same time, our interpretation also underscores the role of molecular friction in controlling the action of eddy fluxes of temperature and salinity. For instance, in the inviscid model ($\nu = 0$), the eddy fluxes would lack the proper phase alignment with the primary wave required for the staircase-induced suppression.

5. Results

The purpose of the section is twofold: (i) the validation of the multiscale theory by DNS in the numerically accessible regime and (ii) the systematic exploration of theory-based predictions over the relevant parameter space.

The first objective is addressed in figure 9, in which theoretical and DNS-based estimates of the decay rate in the diffusive ($s = -1$) regime are plotted as a function of k . The staircase DNS are identical to the one discussed in § 3 (figures 1–3) in all respects except for the wavelengths, which are systematically varied. The four DNS of this type (indicated by the plus signs) assume the horizontal wavelengths of $L_x = 800, 1200, 1600$ and 2000 ; the vertical wavelengths are assigned values $L_z = 0.5L_x$. The decay rates diagnosed from DNS are consistent with the corresponding theoretical estimates, which are indicated by the solid curve. For instance, the multiscale model predicts $\lambda_d = 3.28 \cdot 10^{-3}$ for the case in figures 1–3, which agrees with the DNS-based estimate (3.7) within 30%. This modest difference is attributed to the somewhat *ad hoc* choice

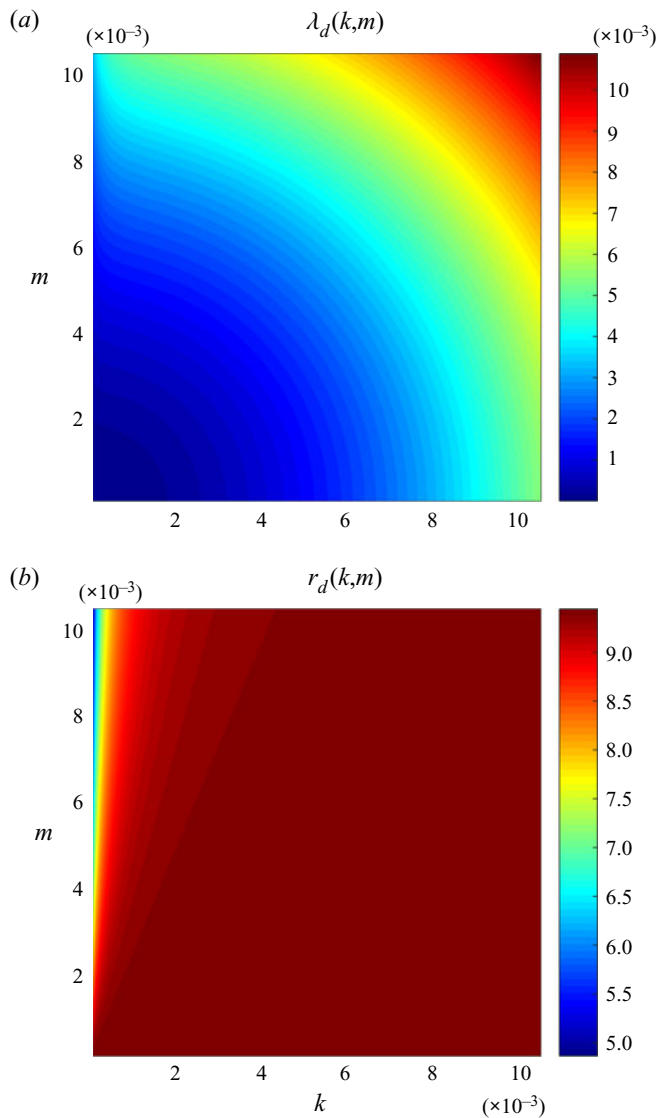


FIGURE 10. The wave decay rate (λ_d) and the attenuation ratio (r_d) realized in the diffusive case are plotted as functions of wavenumbers (k, m) in (a) and (b) respectively.

of the nominal value of relative interfacial height ($h_i = 0.1$) – a free parameter in the theoretical model. The best fit of the theoretical model to DNS suggests $h_i = 0.0688$ and the corresponding pattern of the decay rate is indicated by the grey dash-dot curve. In figure 9, we also show (dashed curve) the theoretical estimate of the wave decay rate in the uniform gradient, which is represented by the term B in (4.25). The corresponding DNS-based estimates are indicated by circles, revealing the remarkable consistency of numerical and theoretical results for linear stratification. Both the multiscale model and DNS suggest that the presence of the staircase increases the decay rates by an order of magnitude.

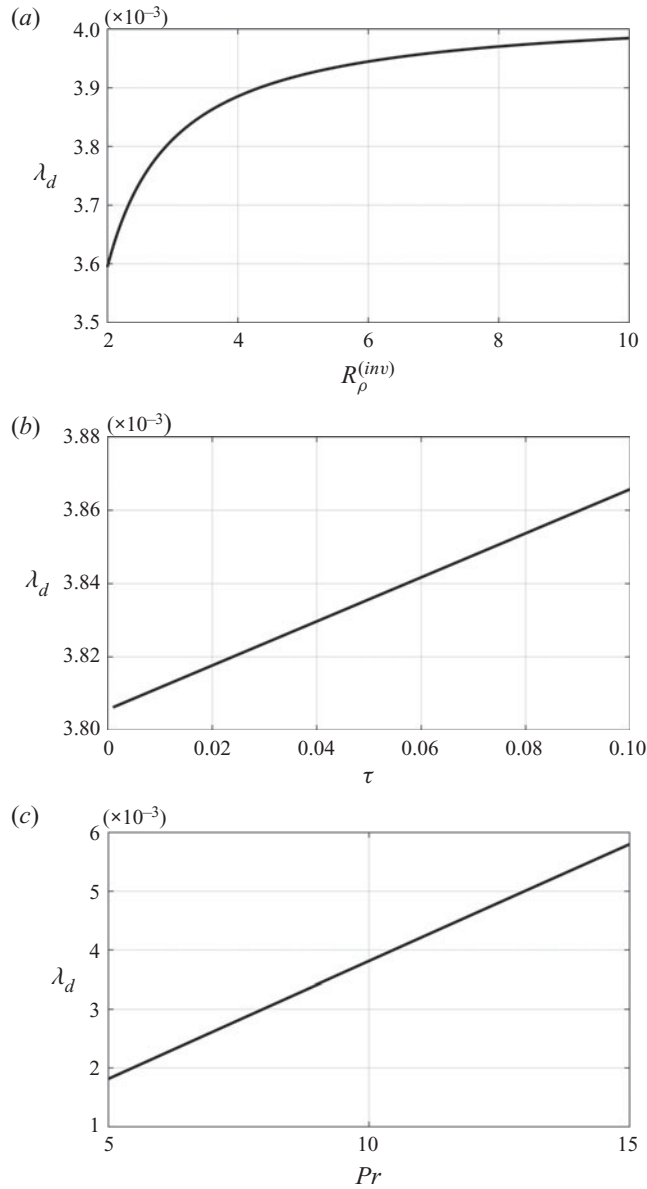


FIGURE 11. The wave decay rate (λ_d) in the diffusive staircase is plotted as a function of (a) the inverse density ratio $R_\rho^{(inv)}$, (b) the diffusivity ratio τ and (c) the Prandtl number Pr .

The comparison of the decay rates in the fingering case ($s = 1$) is also encouraging. The DNS shown in figures 4–6 yields $\lambda_d = 1.55 \cdot 10^{-3}$, whereas the corresponding theoretical estimate (4.27) is $\lambda_d = 2.09 \cdot 10^{-3}$. A reference should be made to 3-D fingering simulations of Stellmach *et al.* (2011), which also reveal the tendency of staircases to suppress internal waves. While those DNS lack the scale separation between steps and waves, they still imply the decay rates of the same order ($\lambda_d \sim 10^{-2}$) as the corresponding theoretical prediction. This qualitative consistency suggests that the

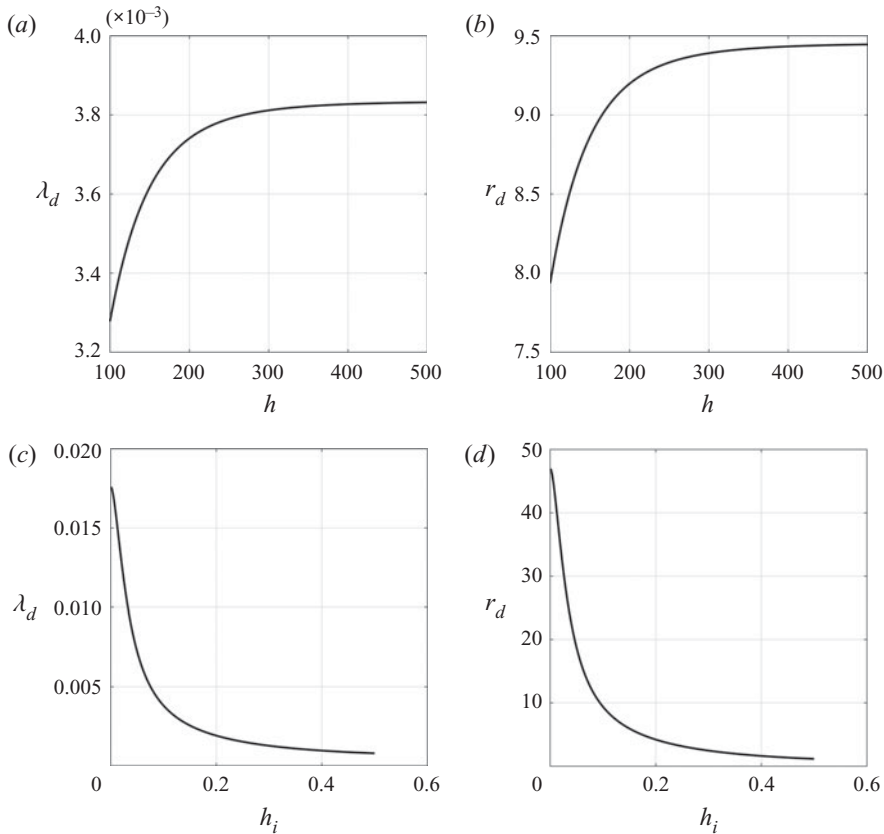


FIGURE 12. The wave decay rate (λ_d) and the attenuation ratio (r_d) realized in the diffusive case are plotted as functions of step height h in (a) and (b), and as functions of the relative interface thickness h_i in (c) and (d).

mechanisms of wave suppression in two and three dimensions are analogous and can be captured by the multiscale models in § 4.

The exploration of the parameter space starts with the analysis of the relation between the decay rates and wavenumbers (k, m), which is shown in figure 10(a). This calculation was performed for the following parameters:

$$R_\rho^{(inv)} = 3, \quad h = 300, \quad h_i = 0.1, \quad Pr = 10, \quad \tau = 0.01, \quad (5.1)$$

which are representative of diffusive staircases in the main Arctic halocline (e.g. Kelley *et al.* 2003; Timmermans *et al.* 2008). The predicted decay rates rapidly and monotonically decrease with the increasing wavenumbers, both vertical and horizontal. The values in figure 10(a) represent the cumulative effect of the staircase-induced and molecular dissipation. Their relative significance is quantified using the attenuation ratio r_d , defined in (4.26). The pattern of $r_d(k, m)$ in figure 10(b) shows that this ratio is fairly uniform, with $r_d \sim 10$ throughout much of the wavenumber space.

Figure 11 examines the dependencies of λ_d on environmental parameters ($R_\rho^{(inv)}, \tau, Pr$). The wavelengths in this calculation are kept at $(L_x, L_z) = (1600, 800)$ and the staircase parameters (h, h_i) are the same as in the baseline configuration (5.1). As one of the parameters ($R_\rho^{(inv)}, \tau, Pr$) is varied, others are assigned fixed values given in (5.1).

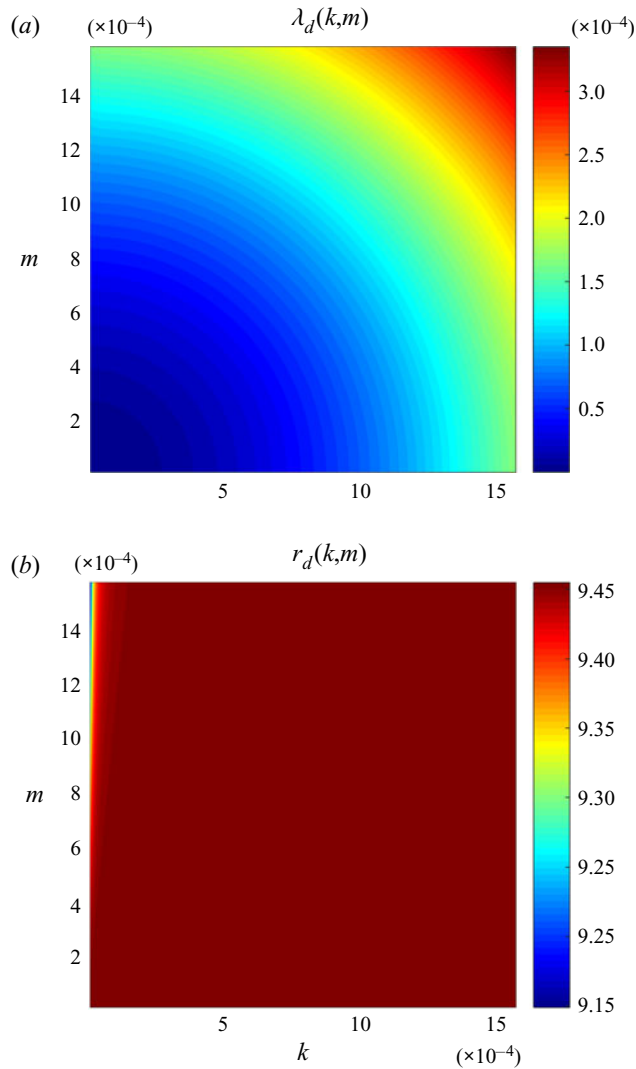


FIGURE 13. The wave decay rate (λ_d) and the attenuation ratio (r_d) realized in the fingering case are plotted as functions of wavenumbers (k, m) in (a) and (b) respectively.

The results in figure 11 indicate that the environmental parameters have a relatively minor impact on the decay rates. The largest variation in λ_d is associated with changes in Pr (figure 11c). However, in much of the World Ocean, the Prandtl number is confined to a relatively narrow interval of $7 < Pr < 13$, and in this range λ_d varies by a factor of two at most.

The dependence of λ_d on staircase characteristics (h, h_i) is explored in figure 12. While the variation in step height h (figure 12a) only weakly influences λ_d , the decay rates are fairly sensitive to the relative thickness of high-gradient interfaces h_i (figure 12c). Low values of h_i , which are realized in sharp well-defined staircases, result in substantially elevated decay rates. Figures 12(b) and 12(d) present the ratio of staircase-induced and molecular attenuation (r_d) as functions of h and h_i respectively. The dependence of this ratio on the step height (h) is weak. However, r_d rapidly increases with decreasing h_i .

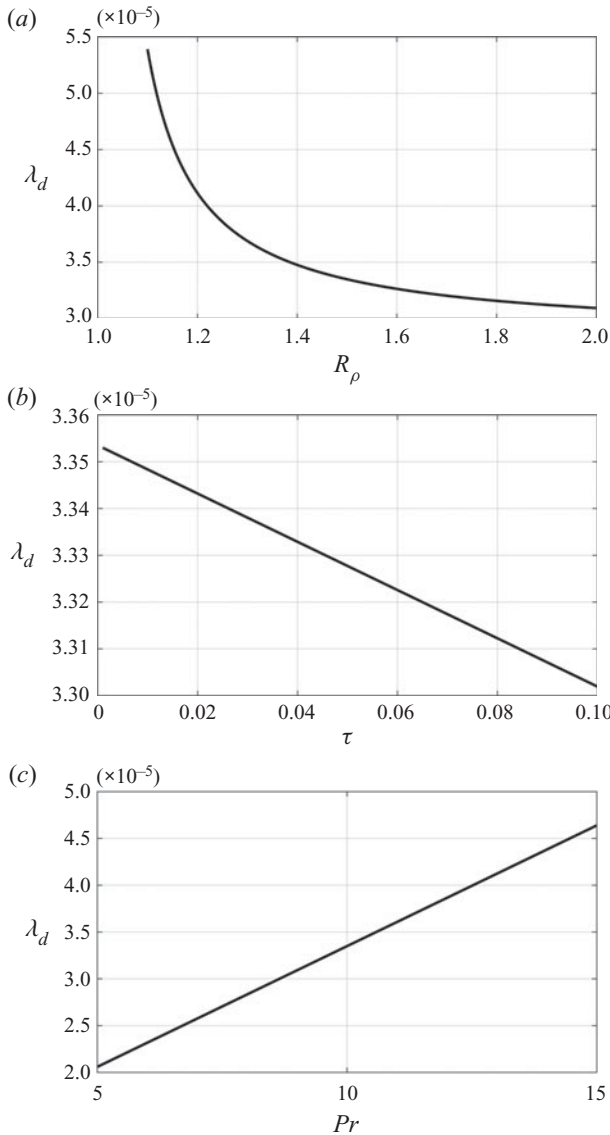


FIGURE 14. The wave decay rate (λ_d) in the fingering staircase is plotted as a function of (a) the density ratio R_ρ , (b) the diffusivity ratio τ and (c) the Prandtl number Pr .

The analysis of decay rates is now reproduced for fingering staircases ($s = 1$). The baseline set of parameters reflects characteristics of the Caribbean staircase (e.g. Schmitt *et al.* 2005)

$$R_\rho = 1.5, \quad h = 2000, \quad h_i = 0.1, \quad Pr = 10, \quad \tau = 0.01. \quad (5.2)$$

Figure 13(a) presents the decay rate pattern, evaluated using (4.27), as a function of wavenumbers. The corresponding attenuation ratio (r_d) is shown in figure 13(b). As previously (cf. figure 10), the decay rate rapidly increases with increasing wavenumbers, whereas the attenuation ratio is remarkably uniform with $r_d \sim 10$. The dependencies

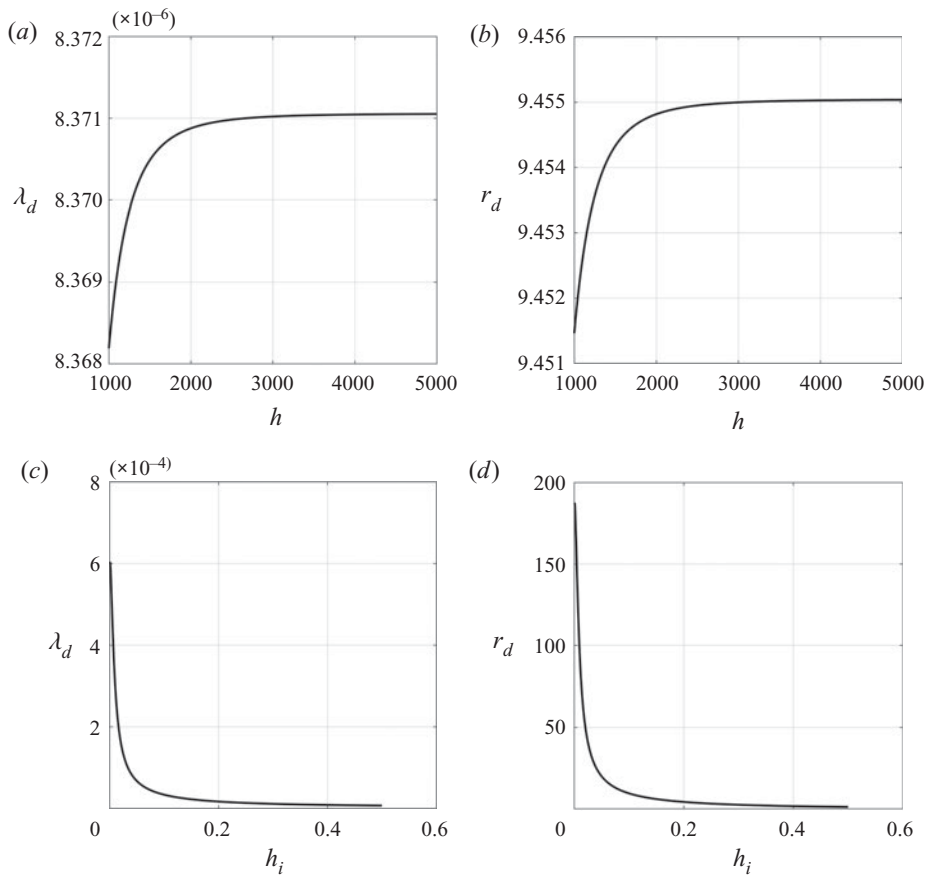


FIGURE 15. The wave decay rate (λ_d) and the attenuation ratio (r_d) realized in the fingering case are plotted as functions of step height h in (a) and (b), and as functions of the relative interface thickness h_i in (c) and (d).

of λ_d on (R_ρ, τ, Pr) , evaluated for $(L_x, L_z) = (2 \cdot 10^4, 10^4)$, are presented in figure 14. These results suggest a limited sensitivity of the decay rates to environmental parameters. Likewise, the influence of the step height on λ_d and r_d is also minimal (figure 15a,b). The variation in the interfacial thickness (h_i), on the other hand, has a substantial impact on both λ_d and r_d (figure 15c,d).

6. Oceanographic implications

The foregoing analysis indicates that the presence of thermohaline staircases tends to suppress free internal waves, but the magnitude of this effect may be limited. This section attempts to offer a more quantitative assessment of the potential ramifications of staircase-induced suppression. To facilitate the interpretation of our results in terms of relevant oceanographic scales, we cast the following discussion in dimensional units. The conversion between the non-dimensional and dimensional quantities is done using representative parameters (2.6). For vertical wavelengths of $\sim 10^3$, which is equivalent to the dimensional scale of $L_z^* \sim 10$ m, both DNS (figure 3) and the multiscale theory (figure 11) predict the decay rate of $\lambda_d \sim 4 \cdot 10^{-3}$. This estimate corresponds to the

dimensional value of $\lambda_d^* \sim 4 \cdot 10^{-6} \text{ s}^{-1}$, representing the e -folding decay periods of 2–3 days. Such intervals are generally less than the time scale of synoptic variability of the atmospheric forcing (2–10 days) and the intrinsic mesoscale variability of the ocean (10–30 days). Thus, it is reasonable to assume that the presence of staircases will adversely affect wave components on vertical scales $L_z^* \sim 10 \text{ m}$. However, the decay rate rapidly (nearly quadratically) decreases with increasing wavelength. Therefore, it seems unlikely that the staircases could have much of an impact on waves with vertical scales exceeding $L_z^* \gtrsim 20 \text{ m}$. On the other hand, the oceanic wave field is dominated by relatively low-order components, with vertical scales of the order of hundreds of metres, generated by the atmospheric forcing and by the interaction of abyssal flows with bathymetry. Thus, the question arises whether the wave-suppression tendency, dynamically interesting as it may be, can substantially influence the oceanic wave environment. Of particular interest is the impact of the staircase-induced suppression on the intensity of irreversible mixing caused by the internal wave overturns.

To address this concern, we turn to the canonical Garrett & Munk (1972) spectrum of internal waves in the ocean, denoted hereafter as GM, which is used to reconstruct the representative time series of vertical shear. Our intent is to determine how the suppression of relatively small-scale waves affects shear and, ultimately, the intensity of small-scale mixing. The implementation is identical to the procedure used by Radko *et al.* (2015) and Radko (2019a). Therefore, only an abbreviated description is given here. The horizontal velocity field is represented by a superposition of internal waves

$$\left. \begin{aligned}
 U^*(z^*, t^*) &= \text{Re} \left[\sum_{j=1}^J \iint a_u(k_{GM}, l_{GM}, j) \cos(m_{GM}(j)z) \right. \\
 &\quad \left. \exp(i(\theta_u(k_{GM}, l_{GM}, j) - \sigma_{GM}t)) dk_{GM} dl_{GM} \right] \\
 V^*(z^*, t^*) &= \text{Re} \left[\sum_{j=1}^J \iint a_v(k_{GM}, l_{GM}, j) \cos(m_{GM}(j)z) \right. \\
 &\quad \left. \exp(i(\theta_v(k_{GM}, l_{GM}, j) - \sigma_{GM}t)) dk_{GM} dl_{GM} \right]
 \end{aligned} \right\}, \tag{6.1}$$

where j represents vertical mode numbers and (k_{GM}, l_{GM}, m_{GM}) are the wavenumbers. The stochastic wave amplitudes (a_u, a_v) conform to the GM internal wave spectrum and have random initial phase distribution. We assume uniform background stratification, and (a_u, a_v) are set to zero for frequencies above the buoyancy frequency N^* and below the Coriolis parameter f^* . The strength of shear is controlled by the maximal vertical mode number J , which is computed by requiring the mean Richardson number

$$Ri_{mean} = \frac{N^{*2}}{[U_z^{*2} + V_z^{*2}]_t}, \tag{6.2}$$

to match the chosen target value; $Ri_{mean} = 1$ is used in the following example. It should be mentioned that wave spectra measured in the upper Arctic Ocean (Levine, Paulson & Morison 1987) are often characterized by a less rapid decrease of spectral energy with

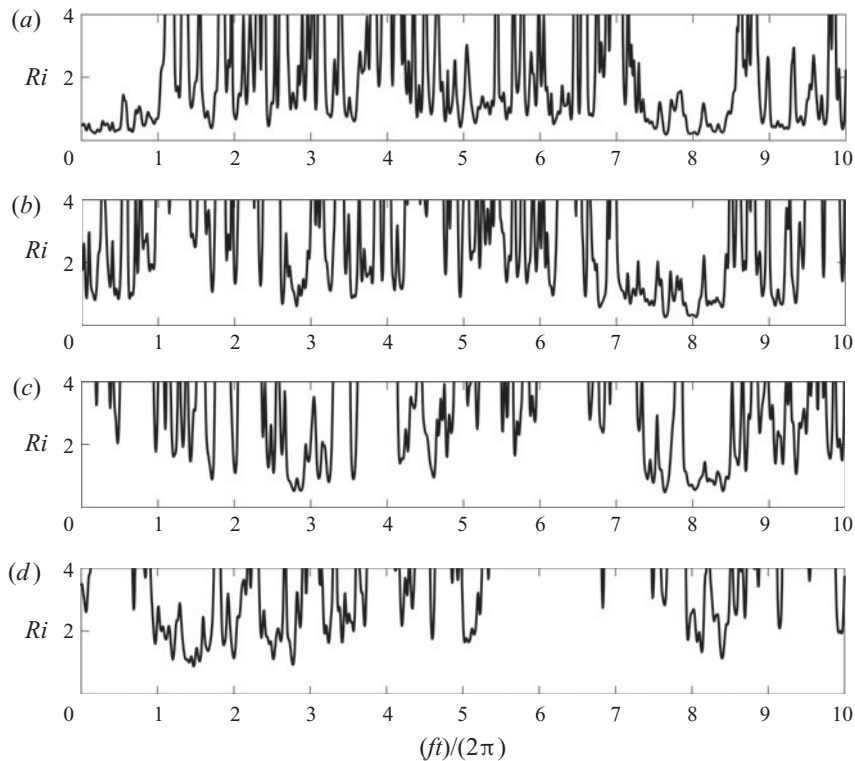


FIGURE 16. Time series of the Richardson number constructed using the GM internal wave spectrum. Time is expressed in terms of inertial periods $2\pi/f$. (a) shows the record of Ri for the canonical GM spectrum. The corresponding records for modified spectra, which retain only wave components with vertical wavelengths exceeding 5 m, 10 m, and 20 m, are presented in (b), (c), and (d) respectively.

frequency than in the GM model. Nevertheless, we find it instructive to perform our preliminary assessment using the canonical GM spectrum.

Using (6.1), the temporal record of shear was reconstructed at the mid-level ($z^* = -500$ m) in the ocean of depth $D = 1000$ m. The calculation was extended in time for ten inertial periods ($2\pi/f^*$) and the results are expressed (figure 16a) in terms of the instantaneous Richardson number $Ri = N^{*2}/(U_z^{*2} + V_z^{*2})$. The Richardson number is traditionally used to determine the susceptibility of shear flows to Kelvin–Helmholtz (KH) instability (von Helmholtz 1868; Kelvin 1871). Non-dissipative flows are KH-unstable if the Richardson number is less than the critical value of $Ri_{cr} = \frac{1}{4}$ (Richardson 1920; Howard 1961; Miles 1961). The amplifying perturbations in this regime tend to evolve into fully turbulent billows (e.g. Woods 1968; Thorpe 1971; Smyth, Moum & Caldwell 2001), which are thought to be one of the principal sources of irreversible diapycnal mixing in the ocean (e.g. Thorpe 2005).

The time series in figure 16(a) indicate that the flow meets the KH instability conditions very intermittently and infrequently, which is consistent with the statistics of the Richardson number derived from the open ocean measurements (e.g. Monin & Ozmidov 1985; Polzin 1996; Polzin *et al.* 2003). Overall, the system spends less than 2% of the time in the unstable regime ($Ri < \frac{1}{4}$). Thus, the question arises whether the staircase-induced suppression of relatively small-scale wave components can substantially

reduce the likelihood of KH destabilization. To investigate this possibility, the calculation in figure 16(a) was modified by suppressing all spectral components in (6.1) with vertical wavelengths smaller than the chosen length scale L_{cr}^* . The resulting time series for $L_{cr}^* = 5$ m, 10 m and 20 m are shown in figure 16(b–d) respectively.

The calculations in figure 16 point to the potentially critical role that small-scale waves play in generating KH overturns. Even the suppression of harmonics with vertical wavelengths $L_z^* < 5$ m (figure 16b) has a major effect on the statistics of the Richardson number. The mean Richardson number increases from $Ri_{mean} = 1.0$ in the original GM model to $Ri_{mean} = 1.91$ and the minimal value increases from $Ri_{min} = 0.18$ to $Ri_{min} = 0.27$. The results for $L_{cr}^* = 10$ m in figure 16(c) are even more dramatic: the average and minimal Richardson numbers increase to $Ri_{min} = 0.49$ and $Ri_{mean} = 2.63$ respectively. Finally, the suppression of waves with $L_z^* < 20$ m (figure 16d) effectively precludes any possibility of KH destabilization: $Ri_{min} = 0.88$ and $Ri_{mean} = 3.90$. These results support our key thesis: the staircase-induced suppression of relatively small-scale waves ($L_z^* \sim 10$ m) could substantially impact the ability of internal waves to generate small-scale turbulence and diapycnal mixing in the ocean.

7. Discussion and conclusions

This study explores the interaction between internal waves and thermohaline staircases, diffusive and fingering, using a combination of DNS and an asymptotic multiscale model. In all cases considered, we find that this interaction results in the systematic weakening of large-scale waves. The simulated wave attenuation is much more intense than could be attributed to the direct influence of molecular friction and diffusion. The multiscale model, which attempts to conceptualize this effect, is validated by DNS in the numerically accessible regime. Particularly encouraging is the finding that the requirement of scale separation between interacting components, which is measured by the parameter ε in (4.2), does not substantially limit the predictive capabilities of the model. For instance, the multiscale theory and DNS produce accurate estimates of the wave decay rates even when its vertical wavelength exceeds the staircase step height by as little as a factor of four. While considerations of analytical tractability led us to explore the limit $\varepsilon \ll 1$, it is important to note that staircases tend to suppress even relatively small-scale waves. For instance, simulations of Stellmach *et al.* (2011) reveal the rapid decay of a wave with the vertical wavelength equal to the step height ($\varepsilon = 1$) after the formation of a staircase.

In our investigation, the multiscale model serves a dual purpose. The inspection of balances that arise at each order in the expansion makes it possible to trace the chain of events leading to wave suppression, providing an unambiguous interpretation of system dynamics. Also important is the opportunity to efficiently explore the wide oceanographically relevant parameter range, most of which is currently inaccessible by DNS even in two dimensions. The damping of internal waves in the multiscale model is associated with eddy diffusion of temperature and salinity on the scale of staircase steps (h). The effects of eddy viscosity, on the other hand, are not reflected at the leading-order theoretical expression of the decay rate. The agreement of the multiscale model and DNS implies that this dynamics is likely to control wave attenuation in more general models and perhaps in the ocean as well. The multiscale theory does not explicitly represent several processes that occur in fully developed staircases, such as convective overturns in the mixed layers and double-diffusive microstructure in the interfaces. Hence, its success indicates that such phenomena play a secondary role in wave/staircase interaction.

In both fingering and diffusive systems, we find that the wave decay rates rapidly increase with increasing wavenumbers, both horizontal and vertical. The sensitivity to

other parameters, including the background density ratio and step height, is limited. The adverse effect of staircases on wave activity is particularly pronounced for intermediate modes with vertical wavelengths that are comparable to the staircase step heights. The anticipated selective filtering of relatively high-order components is likely to reduce the wave-induced vertical shear and, ultimately, limit the magnitude of irreversible diapycnal mixing associated with overturning internal waves. The calculations based on the canonical Garrett–Munk internal wave spectrum (§ 6) support this proposition. The suppression of relatively small-scale waves ($L_z^* < 10$ m) increases the mean and minimal Richardson numbers by approximately a factor of 2.5, which can substantially reduce the probability of overturns and thereby influence the levels of wave-induced mixing.

Interestingly, such a scenario is not inconsistent with oceanographic observations. For instance, diapycnal small-scale mixing in the well-studied fingering Caribbean staircase (Schmitt *et al.* 2005) was shown to be predominantly double diffusive. Likewise, the Arctic halocline, heavily populated by diffusive staircases, is also characterized by relatively low levels of turbulence associated with overturning internal waves (e.g. Guthrie *et al.* 2013, 2015). Of course, there are numerous other reasons to expect limited internal wave activity and wave-induced mixing in the upper Arctic. Commonly invoked explanations include the reduced surface forcing in ice-covered regions, enhanced under-ice dissipation and weak tides with frequencies that lie outside of the range of free internal waves (e.g. Levine, Paulson & Morison 1985; Pinkel 2005; Cole *et al.* 2018). However, the suppression mechanism advocated in the present study could play a contributing role in limiting wave-induced mixing in staircase-rich regions of the World Ocean.

It should be emphasized at this point that the presented analysis is not meant to offer an exhaustive treatment of the problem. The minimalistic design of the asymptotic model, which includes only essential components, is intentional. The choices made were influenced by the considerations of dynamic transparency, and the model can be extended in several promising directions. For instance, the model did not take into account processes that are nonlinear in wave amplitude, which led to a straightforward calculation of linear decay rates. However, this simplification also precluded the analysis of fundamentally nonlinear effects – such as harmonic generation and energy trapping (Wunsch 2018) – that could be potentially significant for higher wave amplitudes. Another interesting question concerns the significance of wave reflection from density interfaces in staircases. In the present configuration, this effect does not play a significant role. Numerical simulations (§ 3) are characterized by low levels of reflected waves, and theory in § 4 also provides no evidence of reflection, attributing suppression to dissipative mechanisms. On the other hand, the model of internal waves incident upon a staircase (Sutherland 2016) attributes the wave attenuation to the reflection from interfaces, ignoring dissipative processes. Hence, new insights can be afforded by a unified theory of suppression that represents both regimes as limiting cases and establishes conditions when these limits are approached.

It is also desirable to develop a three-dimensional counterpart of the multiscale theory that would incorporate planetary rotation and examine the associated changes in staircase-induced suppression. In this regard, it should be stressed that the Coriolis effect undoubtedly affects the dominant large-scale internal waves, remotely generated by surface forcing and flow-bathymetry interactions. However, diapycnal wave-driven mixing requires the presence of high-order modes that are produced through the destabilization of large-scale waves (e.g. parametric instabilities) and nonlinear wave–wave interactions. It is the high-wavenumber part of the spectrum that is most susceptible to the staircase-induced suppression, and for those components, planetary rotation could be of secondary importance. Nevertheless, it is perhaps prudent to view the present version of theory as an attempt to rationalize the wave decay in laboratory experiments (Ruddick 1980, 1985)

and non-rotating DNS (Stellmach *et al.* 2011). In terms of other applications, the proposed model is suggestive and can provide guidance for future studies.

Acknowledgements

Support of the National Science Foundation (grant OCE 1756491) is gratefully acknowledged. The author thanks Neil Balmforth, Justin Brown, and the anonymous reviewers for helpful comments.

Declaration of interests

The author reports no conflict of interest.

REFERENCES

- BALMFORTH, N. J. & YOUNG, Y.-N. 2002 Stratified Kolmogorov flow. *J. Fluid Mech.* **450**, 131–167.
- BALMFORTH, N. J. & YOUNG, Y.-N. 2005 Stratified Kolmogorov flow. Part 2. *J. Fluid Mech.* **528**, 23–42.
- BEBIEVA, Y. & SPEER, K. 2019 The regulation of sea ice thickness by double-diffusive processes in the Ross Gyre. *J. Geophys. Res.: Oceans* **124**, 7068–7081.
- CARPENTER, J. R., SOMMER, T. & WUEST, A. 2012 Simulations of a double-diffusive interface in the diffusive convection regime. *J. Fluid Mech.* **711**, 411–436.
- COLE, S. T., TOOLE, J. M., RAINVILLE, L. & LEE, C. M. 2018 Internal waves in the Arctic: influence of ice concentration, ice roughness, and surface layer stratification. *J. Geophys. Res.: Oceans* **123**, 5571–5586.
- FERNANDO, H. J. S. 1989 Buoyancy transfer across a diffusive interface. *J. Fluid Mech.* **209**, 1–34.
- FLANAGAN, J., LEFLER, A. & RADKO, T. 2013 Heat transport through diffusive interfaces. *Geophys. Res. Lett.* **40**, 2466–2470.
- GAMA, S., VERGASSOLA, M. & FRISCH, U. 1994 Negative eddy viscosity in isotropically forced 2-dimensional flow – linear and nonlinear dynamics. *J. Fluid Mech.* **260**, 95–126.
- GARAUD, P. 2018 Double-diffusive convection at low Prandtl number. *Annu. Rev. Fluid Mech.* **50**, 275–298.
- GARRETT, C. & MUNK, W. 1972 Space-time scales of ocean internal waves. *Geophys. Fluid Dyn.* **3**, 225–264.
- GHAEMSAIDI, S., DOSSER, H. V., RAINVILLE, L. & PEACOCK, T. 2016 The impact of multiple layering on internal wave transmission. *J. Fluid Mech.* **789**, 617–629.
- GUTHRIE, J. D., FER, I. & MORISON, J. 2015 Observational validation of the diffusive convection flux laws in the Amundsen Basin, Arctic Ocean. *J. Geophys. Res.: Oceans* **120**, 7880–7896.
- GUTHRIE, J. D., MORISON, J. H. & FER, I. 2013 Revisiting internal waves and mixing in the Arctic Ocean. *J. Geophys. Res.: Oceans* **118**, 3966–3977.
- VON HELMHOLTZ, H. 1868 Ueber discontinuierliche Flüssigkeits-Bewegungen [On the discontinuous movements of fluids]. *Monatsber. Konigl. Preuss. Akad. Wiss. Berlin* **23**, 215–228.
- HOLYER, J. Y. 1981 On the collective instability of salt fingers. *J. Fluid Mech.* **110**, 195–207.
- HOLYER, J. Y. 1985 The stability of long steady three-dimensional salt fingers to long wavelength perturbations. *J. Fluid Mech.* **156**, 495–503.
- HOWARD, L. N. 1961 Note on a paper of John W. Miles. *J. Fluid Mech.* **10**, 509–512.
- KELLEY, D. E. 1990 Fluxes through diffusive staircases: a new formulation. *J. Geophys. Res.* **95**, 3365–3371.
- KELLEY, D. E., FERNANDO, H. J. S., GARGETT, A. E., TANNY, J. & OZSOY, E. 2003 The diffusive regime of double-diffusive convection. *Prog. Oceanogr.* **56**, 461–481.
- KELVIN, LORD 1871 Influence of wind and capillarity on waves in water supposed frictionless. *Math. Phys. Papers* **4**, 76–85.
- KRISHNAMURTI, R. 2009 Heat, salt and momentum transport in a laboratory thermohaline staircase. *J. Fluid Mech.* **638**, 491–506.

- LEVINE, M. D., PAULSON, C. A. & MORISON, J. H. 1985 Internal waves in the Arctic Ocean: comparison with lower-latitude observations. *J. Phys. Oceanogr.* **15**, 800–809.
- LEVINE, M. D., PAULSON, C. A. & MORISON, J. H. 1987 Observations of internal gravity waves under the Arctic pack ice. *J. Geophys. Res.* **92** (C), 779–782.
- LINDEN, P. F. & SHIRTCLIFFE, T. G. L. 1978 The diffusive interface in double-diffusive convection. *J. Fluid Mech.* **87**, 417–432.
- MANFROI, A. & YOUNG, W. 1999 Slow evolution of zonal jets on the beta plane. *J. Atmos. Sci.* **56**, 784–800.
- MANFROI, A. & YOUNG, W. 2002 Stability of beta-plane Kolmogorov flow. *Physica D* **162**, 208–232.
- MEI, C. C. & VERNESCU, M. 2010 *Homogenization Methods for Multiscale Mechanics*. World Scientific.
- MESHALKIN, L. & SINAI, Y. 1961 Investigation of the stability of a stationary solution of a system of equations for the plane movement of an incompressible viscous fluid. *J. Appl. Math. Mech.* **25**, 1700–1705.
- MILES, J. W. 1961 On the stability of heterogeneous shear flows. *J. Fluid Mech.* **10**, 496–508.
- MONIN, A. S. & OZMIDOV, R. V. 1985 *Turbulence in the Ocean*. D. Reidel.
- NOVIKOV, A. & PAPANICOLAOU, G. 2001 Eddy viscosity of cellular flows. *J. Fluid Mech.* **446**, 173–198.
- PINKEL, R. 2005 Near-inertial wave propagation in the western Arctic. *J. Phys. Oceanogr.* **35**, 645–665.
- POLYAKOV, I. V., *et al.* 2017 Greater role for Atlantic inflows on sea-ice loss in the Eurasian Basin of the Arctic Ocean. *Science* **356**, 285–291.
- POLZIN, K. 1996 Statistics of the Richardson number: mixing models and fine structure. *J. Phys. Oceanogr.* **26**, 1409–1425.
- POLZIN, K. L., KUNZE, E., TOOLE, J. M. & SCHMITT, R. W. 2003 The partition of fine-scale energy into internal waves and geostrophic motions. *J. Phys. Oceanogr.* **33**, 234–248.
- RADKO, T. 2008 The double-diffusive modon. *J. Fluid Mech.* **609**, 59–85.
- RADKO, T. 2011 Eddy viscosity and diffusivity in the modon-sea model. *J. Mar. Res.* **69**, 723–752.
- RADKO, T. 2013 *Double-Diffusive Convection*. Cambridge University Press.
- RADKO, T. 2014 Applicability and failure of the flux-gradient laws in double-diffusive convection. *J. Fluid Mech.* **750**, 33–72.
- RADKO, T. 2019a Thermohaline-shear instability. *Geophys. Res. Lett.* **46**, 822–832.
- RADKO, T. 2019b Thermohaline layering on the microscale. *J. Fluid Mech.* **862**, 672–695.
- RADKO, T., BALL, J., COLOSI, J. & FLANAGAN, J. 2015 Double-diffusive convection in a stochastic shear. *J. Phys. Oceanogr.* **45**, 3155–3167.
- RICHARDSON, L. F. 1920 The supply of energy from and to atmospheric eddies. *Proc. R. Soc. A* **97**, 354–373.
- RUDDICK, B. R. 1980 Stress at a sheared finger interface. In *Hydraulics and Fluid Mechanics Conference*. Institution of Engineers.
- RUDDICK, B. R. 1985 Momentum transport in thermohaline staircases. *J. Geophys. Res.* **90**, 895–902.
- SCHMITT, R. W. 1994 Double diffusion in oceanography. *Annu. Rev. Fluid Mech.* **26**, 255–285.
- SCHMITT, R. W., LEDWELL, J. R., MONTGOMERY, E. T., POLZIN, K. L. & TOOLE, J. M. 2005 Enhanced diapycnal mixing by salt fingers in the thermocline of the tropical Atlantic. *Science* **308**, 685–688.
- SMYTH, W., MOUM, J. & CALDWELL, D. 2001 The efficiency of mixing in turbulent patches: inferences from direct simulations and microstructure observations. *J. Phys. Oceanogr.* **31**, 1969–1992.
- STELLMACH, S., TRAXLER, A., GARAU, P., BRUMMEL, N. & RADKO, T. 2011 Dynamics of fingering convection II: the formation of thermohaline staircases. *J. Fluid Mech.* **677**, 554–571.
- STERN, M. E. 1960 The “salt-fountain” and thermohaline convection. *Tellus* **12**, 172–175.
- STERN, M. E. 1969 Collective instability of salt fingers. *J. Fluid Mech.* **35**, 209–218.
- STERN, M. E., RADKO, T. & SIMEONOV, J. 2001 3D salt fingers in an unbounded thermocline with application to the Central Ocean. *J. Mar. Res.* **59**, 355–390.
- SUTHERLAND, B. R. 2016 Internal wave transmission through a thermohaline staircase. *Phys. Rev. Fluids* **1**, 013701.
- THORPE, S. A. 1971 Experiments on instability and turbulence of stratified shear flows: miscible fluids. *J. Fluid Mech.* **46**, 299–319.
- THORPE, S. A. 2005 *The Turbulent Ocean*. Cambridge University Press.

- TIMMERMANS, M.-L., TOOLE, J., KRISHFIELD, R. & WINSOR, P. 2008 Ice-tethered profiler observations of the double-diffusive staircase in the Canada Basin thermohaline. *J. Geophys. Res.* **113**, C00A02.
- TRAXLER, A., STELLMACH, S., GARAUD, P., RADKO, T. & BRUMMEL, N. 2011 Dynamics of fingering convection I: small-scale fluxes and large-scale instabilities. *J. Fluid Mech.* **677**, 530–553.
- TURNER, J. S. 1985 Multicomponent convection. *Annu. Rev. Fluid Mech.* **17**, 11–44.
- TURNER, J. S. 2010 The melting of ice in the Arctic Ocean: the influence of double-diffusive transport of heat from below. *J. Phys. Oceanogr.* **40**, 249–256.
- VERONIS, G. 2007 Updated estimate of double diffusive fluxes in the C-SALT region. *Deep-Sea Res. I* **54**, 831–833.
- WOODS, J. D. 1968 Wave-induced shear instability in the summer thermocline. *J. Fluid Mech.* **32**, 791–800.
- WORSTER, M. G. 2004 Time-dependent fluxes across double-diffusive interfaces. *J. Fluid Mech.* **505**, 287–307.
- WUNSCH, S. 2018 Nonlinear harmonic generation by internal waves in a density staircase. *Phys. Rev. Fluids* **3**, 114803.